3274–3293 *Nucleic Acids Research, 2021, Vol. 49, No. 6* *Published online 8 March 2021*
doi: 10.1093/nar/gkab150

Binding site profiles and N-terminal minor groove interactions of the master quorum-sensing regulator LuxR enable flexible control of gene activation and repression

Jun Zhang[1,†], Bing Liu[5,†], Dan Gu[6,†], Yuan Hao[1], Mo Chen[1], Yue Ma[1], Xiaohui Zhou[7], David Reverter[5,*], Yuanxing Zhang[1,3,4] and Qiyao Wang[1,2,4,*]

[1]State Key Laboratory of Bioreactor Engineering, East China University of Science and Technology, Shanghai 200237, China, [2]Laboratory for Marine Fisheries Science and Food Production Processes, Qingdao National Laboratory for Marine Science and Technology, Qingdao, China, [3]Southern Marine Science and Engineering Guangdong Laboratory (Zhuhai), 519000 Zhuhai, China, [4]Shanghai Engineering Research Center of Maricultured Animal Vaccines, Shanghai, China, [5]Institut de Biotecnologia i Biomedicina, Dept. de Bioquímica i Biologia Molecular, Universitat Autònoma de Barcelona, 08193 Bellaterra, Spain, [6]Jiangsu Key Laboratory of Zoonosis/Jiangsu Co-Innovation Center for Prevention and Control of Important Animal Infectious Diseases and Zoonoses, Yangzhou University, Yangzhou 225009, China and [7]Department of Pathobiology and Veterinary Science, University of Connecticut, Storrs, CT 06269, USA

Received October 29, 2020; Revised February 19, 2021; Editorial Decision February 22, 2021; Accepted February 23, 2021

ABSTRACT

LuxR is a TetR family master quorum sensing (QS) regulator activating or repressing expression of hundreds of genes that control collective behaviors in *Vibrios* with underlying mechanism unknown. To illuminate how this regulator controls expression of various target genes, we applied ChIP-seq and DNase I-seq technologies. *Vibrio alginolyticus* LuxR controls expression of ∼280 genes that contain either symmetric palindrome (repDNA) or asymmetric (actDNA) binding motifs with different binding profiles. The median number of LuxR binding sites for activated genes are nearly double for that of repressed genes. Crystal structures of LuxR in complex with the respective repDNA and actDNA motifs revealed a new mode of LuxR DNA binding that involves contacts of its N-terminal extension to the minor groove. The N-terminal contacts mediated by Arginine-9 and Arginine-11 differ when LuxR binds to repDNA vs actDNA, leading to higher binding affinity at repressed targets. Moreover, modification of LuxR binding sites, binding profiles, and N-terminal extension have important consequences on QS-regulated phenotypes. These results facilitate fundamental understanding of the high flexibility of mechanisms of LuxR control of gene activation and repression in *Vibrio* QS, which may facilitate to design QS inhibiting chemicals that interfere with LuxR regulation to effectively control pathogens.

INTRODUCTION

Quorum sensing (QS) is a cell-to-cell communicating system widely employed by bacteria to regulate numerous genes' expression in response to the accumulated extracellular signaling molecules called autoinducers (1). In the model QS bacterium *Vibrio harveyi*, a critical-threshold high concentration of autoinducers could trigger sophisticated transmembrane signaling that culminates to the control of LuxR, the master QS regulator (MQSR) and LuxR-mediated expression of genes required for group behaviors such as biofilm formation, motility, bioluminescence and pathogenesis (2,3).

Most vibrios adopt *V. harveyi*-like QS cascades and depend on conserved MQSR LuxR homologs, including LuxR (*V. harveyi*), HapR (*V. cholerae*), SmcR (*V. vulnificus*), and OpaR (*V. parahaemolyticus*) for a wide range of QS outputs (4–6). LuxR homologs are unique TetR family transcription factors with a characteristic helix-turn-helix (HTH) DNA binding motif in the N-terminal domain (4,7).

*To whom correspondence should be addressed. Tel: +86 21 64253306; Email: oaiwqiyao@ecust.edu.cn
Correspondence may also be addressed to David Reverter. Tel: +34 93 5868955; Email: David.Reverter@uab.cat
†The authors wish it to be known that, in their opinion, the first three authors should be regarded as Joint First Authors.

In *V. harveyi*, the LuxR-binding motif in repressed promoters has a dyad symmetry, whereas the motif in activated promoters is an incomplete palindrome (8). Similarly, two distinct binding motifs have also been identified for HapR-regulated genes in *V. cholerae* (9). The alignment of the sequences for SmcR binding revealed a 22-bp consensus sequence (10). The apo protein crystals of HapR and SmcR have been resolved (5,6). Despite the knowledge of LuxR homologs in the regulation of QS genes, the molecular basis and mechanisms of LuxR protein action in simultaneously controlling the expression of hundreds of genes via their direct activation or repression on regulated promoters remain unknown.

Vibrio alginolyticus is a marine-born opportunistic pathogenic bacterium, causing severe soft tissue infections, sepsis and ear infections in human and high-mortality diseases in aquatic animals in summer (11). In *V. alginolyticus*, *V. harveyi*-like QS systems have been identified that harbor three parallel systems and transmit signals via two-component system-mediated phosphorelay that ultimately converge information at the regulatory protein LuxO (12,13). The AI-1 signal is synthesized by LuxM and recognized by LuxN (14,15). The LuxS/PQ system utilizes the signal molecule AI-2 and the precursor of AI-2 is synthesized by LuxS (12,16). The signal molecule CAI-1 is dependent on CqsA for its synthesis and detected by CqsS (17). At low cell density (LCD), an insufficient concentration of signal molecules drives the sensors to function as kinases, and the phosphorylated LuxO leads to the lowest expression of LuxR. However, at high cell density (HCD), the high concentration of signal molecules triggers the transfer of phosphate groups, and the dephosphorylated LuxO protein is inactivated to reduce the level of inhibiting sRNA *qrr*s, and eventually LuxR production is enhanced (Figure 1A) (12,18,19).

The transcription of *luxR* itself is controlled by the HCD- and LCD-induced MQSRs LuxR and AphA, respectively (18,19). These two factors, along with other transcriptional factors, i.e. RpoE and VqsA, bind to the *luxR* promoter region and constitute a complicated regulatory network that enables the integration of AI signals and various physiological and environmental signals to control *luxR* transcription and QS outputs, thus coordinating the expression of virulence factors, including the exotoxin Asp, hemolysin, extracellular products, lipopolysaccharides, siderophore, secretion systems and biofilm (20–27), but the molecular mechanisms by which LuxR controls the large regulon are still unclear in *V. alginolyticus* and other vibrios.

Here, we found that LuxR protein in *V. alginolyticus* is the core element for the QS at high cell density. High-resolution DNase I footprinting and sequencing (DNase I-seq) technology was used to determine the binding motifs and binding profiles of LuxR in the activated and repressed promoters, respectively. Furthermore, the crystallization of LuxR in complex with the DNA motifs revealed unique binding mechanisms of the N-terminal LuxR-arm domain with minor grooves, which determines the different binding affinities for repression and activation motifs. We also showed that LuxR binding site sequence, location, and N-terminal extension interactions altogether contribute to the gene repression and activation flexibility of *Vibrio* QS. Collectively, the data from this study provides fundamental molecular insights into the QS regulation mechanisms in vibrios.

MATERIALS AND METHODS

Bacterial stains and culture conditions

The strains and plasmids used in this study are listed in Supplementary Table S1. All strains were constructed as previously described using specific primers (Supplementary Table S2) and isothermal assembly (28). *Vibrio alginolyticus* strains and derivatives were typically grown at 30°C in Luria-Bertani (LB) medium supplemented with 3% NaCl (LBS). *Escherichia coli* strains were grown at 37°C in LB medium. When appropriate, the medium was supplemented with carbenicillin (100 μg/ml), chloramphenicol (25 μg/ml), kanamycin (50 μg/ml), IPTG (1 mmol/L) or L-arabinose (0.04%, w/v).

Plasmids, strains and mutants

The full-length LuxR gene was cloned from the *V. alginolyticus* genome. Different constructs of LuxR were amplified by PCR and cloned in to the BamHI/XhoI restriction enzyme sites of a pET28 vector using ligation-dependent cloning for expression with an N-terminal hexa-histidine (His_6) tag for nickel affinity purification. Point mutations were generated using a QuickChange site-directed mutagenesis Kit (Stratagene).

Protein expression and purification

pET28 vectors harboring different constructs of LuxR were transformed into *E. coli* BL21(DE3) cells, and the expression was induced with 0.5 mM isopropyl β-D-1-thiogalactopyranoside and grown overnight at 20°C. LuxR proteins were purified by nickel affinity chromatography using a buffer containing 300 mM NaCl, 20 mM Tris–HCl, pH 8.0, and 1 mM dithiothreitol (DTT) and eluted with a similar buffer containing 300 mM imidazole. After His_6 removal using thrombin, LuxR proteins were further purified by gel filtration (Superdex 75 column, GE Healthcare) chromatography pre-equilibrated in 300 mM NaCl, 20 mM Tris–HCl, pH 8.0, 1 mM DTT. The selenomethionine (SeMet)-labeled LuxR was expressed in the *E. coli* B834(DE3) strain in M9 medium. The purification steps for the SeMet-labeled LuxR were similar to those used for the native protein.

Crystallization, data collection and structure determination

All complementary single-stranded DNA oligonucleotides of actDNA (5′-ATAATGACATTACTGTATATA-3′) and repDNA (5′-TTATTGATAAAATTATCAATA-3′) were annealed to duplex strands in buffer containing 50 mM NaCl, 10 mM Tris–HCl, pH 8.0, and 1 mM EDTA. LuxR and SeMet-labeled LuxR were concentrated to 876 μM and 771 μM for crystallization. LuxR-DNA complexes were prepared by mixing LuxR with duplex DNA oligonucleotides at a 1:1.2 molar ratio. Diffraction quality crystals

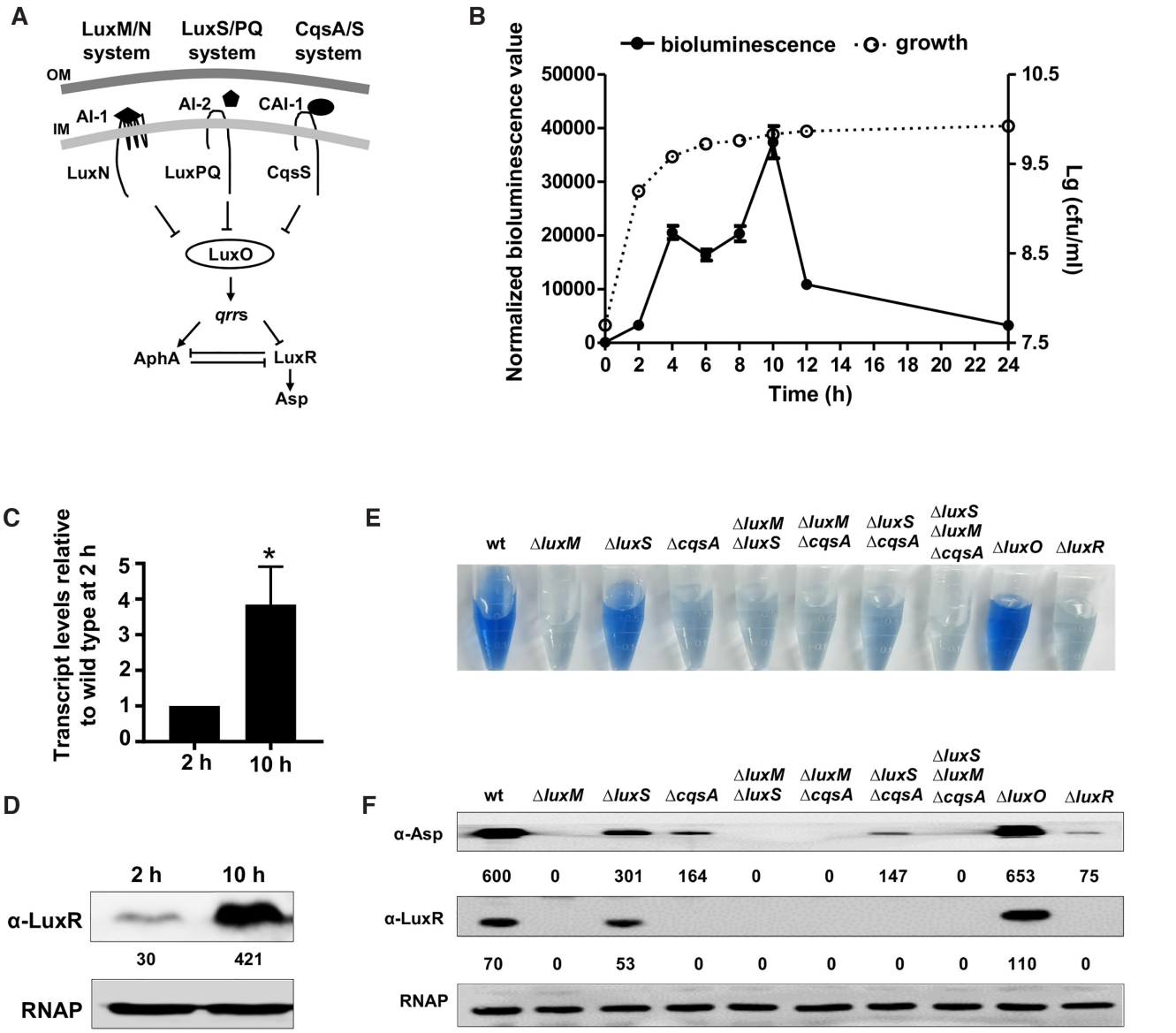

Figure 1. LuxR is involved in QS regulation in *V. alginolyticus*. (**A**) QS systems in *V. alginolyticus*. At HCD, QS autoinducers AI-1, AI-2 and CAI-1 produced by LuxM, LuxS and CqsA, respectively, are sensed by corresponding histidine kinases to trigger signaling cascades and control the yields of MQSR AphA and LuxR which regulates exotoxin Asp and other various QS genes. The lines with arrows indicate positive regulation and bar-ended lines for negative regulation. (**B**) Growth of *V. alginolyticus* and *luxR* transcriptional levels. The transcriptional activity of *luxR* was determined by the P_{luxR}-*luxAB* reporter with the *luxR* promoter fused to promoterless *luxAB*. The relative bioluminescence value was normalized by the CFU. (**C**, **D**) qRT-PCR (C) and western blot (D) analyses of the expression level of *luxR* at 2 h (LCD) and 10 h (HCD). The assays were performed in triplicate. $^*P < 0.05$ (Student's *t*-test). The numbers indicate the densitometric analysis of the bands. (**E**, **F**) HPA digestion assays (E) and western blot analysis (F) were used to determine the levels of extracellular Asp and cellular LuxR in the QS mutant strains. RNAP was used as the loading control.

were obtained by hanging drop with vapor diffusion after 2–3 days using solutions containing 50 mM sodium formate, 50 mM Tris–HCl, pH 7.5, 22% PEG 2000 MME for LuxR-actDNA; 50 mM bis–tris propane, pH 7.5, 20% PEG 2000 MME for LuxR-repDNA, 50 mM sodium formate, 50 mM bis–tris propane pH 7.5; and 16% PEG 2000 MME for SeMet-labeled LuxR-repDNA. A single crystal was soaked in a well solution supplemented with 25% ethylene glycol (v/v) and flash-frozen in liquid nitrogen for data collection. Native and SeMet-labeled datasets were collected at ALBA synchrotron in Barcelona (BL13-XALOC beamline) (29), and processed with XDS (30) and scaled, reduced and further analyzed using CCP4 (31). The heavy atom sites and initial density map were calculated using PHENIX SAD Autosol (32). After an initial automated build, the model was manually built and corrected in Coot (33). This initial model was used as a search model for molecular replacements in the native dataset with Phaser-Phenix (34). The final model for the native dataset was manually reconstructed using Coot (33) and further refined with PHENIX (32). More details on the data collection process and refinement statistics are shown in Table 1.

Table 1. Data collection and structure refinement statistics

Data collection	LuxR-actDNA (native)	LuxR-repDNA (native)	LuxR-repDNA (SeMet-Peak)
Beamline	ALBA-XALOC	ALBA-XALOC	ALBA-XALOC
Space group	*P* 41	*P* 41	*P* 41
Wave length (Å)	0.91918	0.97903	0.97903
Resolution (Å)	61.966–2.543 (2.552–2.543)	61.603–2.236 (2.244–2.236)	69.579–2.551 (2.560–2.551)
a, *b*, *c* (Å)	68.91, 68.91, 123.93	69.34, 69.34, 123.21	69.58, 69.58, 125.76
α, β, γ (°)	α = β = γ = 90	α = β = γ = 90	α = β = γ = 90
Unique reflections	18 962	28 010	19 443
Data redundancy	13.7 (13.9)	5.0 (5.3)	13.7 (13.4)
R_{merge}	0.135 (1.910)	0.055 (1.350)	0.095 (2.990)
CC (1/2)	0.984 (0.581)	0.999 (0.460)	0.998 (0.613)
I/σ	11.3 (1.5)	15.3 (1.4)	16.5 (1.0)
Completeness (%)	99.7 (100.0)	96.4 (98.2)	99.8 (100.0)
Refinement			
Resolution (Å)	60.223–2.600	49.030–2.300	
Non-anomalous reflections	17 742	25 723	
R_{work}/R_{free}	0.2216/0.2492	0.2115/0.2424	
Number of all atoms	3850	3928	
RMSD bond (Å)/angle (°)	0.004/0.792	0.005/0.005	
Ramachandran plot			
Favored (%)	94.99	96.71	
Allowed (%)	5.01	3.29	
Disallowed (%)	0.00	0.00	

Total RNA extraction

Bacteria were incubated at 30°C and harvested after 2 h (LCD) and 10 h (HCD). Total RNA was isolated using an RNA extraction kit (Tiangen, Beijing, China). The RNA samples were digested with DNase I (Promega, Madison, WI, USA) to eliminate genomic DNA contamination.

Quantitative real-time reverse transcription PCR (qRT-PCR)

Equal amounts of RNA (1 μg) were used to generate complementary DNA (Toyobo, Tsuruga, Japan) using random primers. Three independent qRT-PCR experiments were performed, and each was run in triplicate on an Applied Biosystems 7500 Real Time System (Applied Biosystems). The specific primer pairs used are shown in Supplementary Table S2. Transcript levels were normalized to 16 sRNA in each sample using the $\Delta\Delta C_T$ method.

RNA-seq transcriptome generation and data analysis

rRNA was removed from 1–5 μg of total RNA using a RiboZero kit for Gram-negative bacteria (Epicentre, Chicago, IL, USA). First-strand cDNA synthesis from rRNA-depleted samples was performed using a TruSeq RNA sample Prep kit (Illumina, San Diego, CA, USA). cDNA was purified using an RNA Clean and Concentrator-25 kit (Zymo Research, Irvine, CA, USA). After second-strand synthesis, the reactions products were cleaned up using AMPure XP beads according to the manufacturer's instructions. The VAHTS Stranded mRNA-seq Library Prep Kit for Illumina (Vazyme, Nanjing, China) was used in the construction of strand-specific RNA-seq libraries. The libraries were sequenced on a HiSeq 2000 platform (Illumina, San Diego, CA, USA), yielding 100-base paired-end reads. Then, the BWA (35) program was used to align the remaining reads to the reference sequences of *V. alginolyticus* 12G01. The number of reads that was mapped to each gene was determined using Picard tools (http://broadinstitute.github.io/picard/faq.html) and then normalized to the reads per kilobase of genic region per million mapped reads (RPKM) to obtain the relative level of expression. ANOVA was performed to analyze the average expression levels of the three biological replicates to determine the one which showed differential expression between any two conditions that were tested (FDR-value < 0.25 and 2-fold change).

Electrophoretic mobility shift assays (EMSAs)

For the electrophoretic mobility shift assays (EMSAs), purified His_6-tagged LuxR was incubated with different Cy5-labeled DNA probes (Supplementary Table S2) in 20 μl of loading buffer (300 mM NaCl, 20 mM Tris–HCl (pH 8.0), 1 mM DTT, and 5%(V/V) glycerol). After the mixture was incubated at 25°C for 30 min, the samples were resolved using 6% polyacrylamide gel electrophoresis in 0.5× TBE (Tris/boric acid/EDTA) buffer on ice at 100 V for 90 min. Then, the gels were scanned using a Typhoon FLA 9500 (GE healthcare, Uppsala, Sweden).

DNase I footprinting assays

Dye primer-based DNase I footprinting assays were performed as previously described (36). Briefly, the promoter regions of RS20495, RS11155, RS21790 (*ppkA2*) and RS21705 (*hcp2*) were amplified by PCR using *pfu* DNA polymerase (Supplementary Table S2) and 6-FAM labeled at the 5′ end. For each assay, 400 ng of the probes were incubated with different amounts of LuxR in a total volume of 40 μl. After the mixture was incubated for 30 min at 25°C, a 10-μl aliquot of a solution containing approximately 0.015 U DNase I (Promega) and 100 nmol of freshly prepared $CaCl_2$ was added. The mixture was then incubated for 1 min at 25°C. The reaction was stopped by adding 140 μl of DNase I stop solution (36). The samples were first ex-

tracted using phenol/chloroform and then precipitated using ethanol, and the pellets were dissolved in 10 μl of MiniQ water. Approximately 2 μl of digested DNA was added to 7.9 μl of HiDi formamide (Applied Biosystems) and 0.1 μl of GeneScan-500 LIZ size standards (Applied Biosystems). The samples were analyzed using a 3730 DNA Analyzer with a G5 dye set that was run with an altered default genotyping module that increased the injection time to 30 s and the injection voltage to 3 kV. The results were analyzed using GeneMapper 4.0 (Applied Biosystems).

Chromatin immunoprecipitation (ChIP), quantitative PCR (ChIP-qPCR), and ChIP-seq

ChIP was performed as previously described (27). Δ*luxR* cells harboring pBAD33::LuxR-*flag* and pBAD33::*flag* were harvested and treated in 1% formaldehyde at room temperature for 10 min incubation. The bacteria were then washed twice with cold PBS and resuspended in 5 ml of SDS lysis buffer (27). Then, the bacteria were sonicated for DNA fragmentation to 100–500 bp at 200 W. The supernatant was used as the input sample. Both the input and the IP samples were washed with 50 μl of protein G beads. The IP samples were then incubated overnight with 50 μl Flag-beads (Sigma-Aldrich, St. Louis, MO, USA). The beads were sequentially washed twice using low-salt wash buffer, high-salt wash buffer, LiCl wash buffer, and TE buffer (27). The beads were then resuspended in 200 μl of elution buffer (27), incubated at 65°C for 2 h. The supernatants containing the immunoprecipitated DNA were collected, and 8 μl of 5 M NaCl was added to all of the IP and input tubes followed by incubation at 65°C overnight to reverse the DNA-protein crosslinking. After treatment with RNase A and proteinase K, ChIP DNA was purified using phenol-chloroform.

ChIP-qPCR was performed with the purified DNA and specific primers (Supplementary Table S2). The enrichment of DNA targets was calculated using the following $\Delta\Delta C_T$ method. For each DNA target, ΔC_T of the input fraction and IP fraction was calculated for both the pBAD33::*flag*/wt and pBAD33::LuxR-*flag*/Δ*luxR* samples. Each value was then divided by the corresponding ΔC_T that was obtained for the nonspecific *gyrB* intragenic region in the strains. Then, the enrichment ratio was calculated from the $\Delta\Delta C_T$ value of the wt strain divided by that of the Δ*luxR* strain.

ChIP-seq was performed with the purified ChIP DNA fragment. Sequencing libraries were constructed with the VAHTATM Turbo DNA library Prep Kit (Vazyme) and subjected to sequencing with a MiSeq sequencer (Illumina). The following analysis was performed as previously described with default parameters (18). Briefly, ChIP-seq reads were mapped to the *V. alginolyticus* 12G01 genome (18). Binding peaks were called using MACS software (37), followed by MEME analysis (http://meme-suite.org) to generate a representative LuxR-binding logo with 'strand only', 'palindrome only' search mode or default parameters.

DNase I-seq

DNase I-seq was performed in a manner similar to ChIP-seq with DNase I added to remove the unprotected DNA. Briefly, after the DNA was fragmented to 100–500 bp, 12 μl of DNase I (0.3 U/μl) was added to 120 μl of fragmented DNA solution and incubated at 25°C for 10 min, then 330 μl of EDTA (50 mM) was added to the mix and incubated at 55°C for 1 min. The subsequent steps and analysis were the same to those used for ChIP-seq. We identified the genes overlapped in the DNase I-seq and RNA-seq analyses, and divided them into activated genes and repressed genes. Then we used each promoter sequence of the activated and repressed genes Blast against the trimmed reads of the DNase I-seq to identify the number of binding sites of each promoter. The transcriptional start sites (TSS) was predicted by the Softberry-BPROM algorithm (http://www.softberry.com) and manually checked with the strand-specific RNA-seq determined TSS.

Bioluminescence and fluorescence assays

The bioluminescence assay was performed as previously described (26). In brief, the overnight culture of reporter strain P_{luxR}-*luxAB*/WT was diluted to 5×10^6 CFU/ml in fresh LBS medium and then incubated at 30°C with shaking at 200 rpm. A 200-μl aliquot was sampled every 2 h for 12 h, and after the addition of 1% decanal, the bioluminescence was measured in an Orion II bioluminescence reader (Berthold Detection Systems, Pforzheim, Germany). In addition, the cultures were sampled, and the cells on the plates were counted to normalize the bioluminescence values of each time point sample.

For the fluorescence assays, cultures were incubated overnight and then diluted 1:100 in fresh LBS medium. After 9 h of growth with shaking at 30°C, the bacterial cells were washed twice with PBS. Then, EGFP fluorescence was measured using a florescence plate reader (BioTek, Winooski, VT, USA).

Extracellular protease activity assay (HPA)

ECP activity was determined using hide powder azure (HPA) (Sigma-Aldrich) digestion as previously described (12). Briefly, the strains were grown in LBS medium at 30°C for 9 h. The cell density was measured at 600 nm (OD_{600}). The bacterial cultures were centrifuged, and the supernatants were then filtered through 0.22-μm filters (Millipore, Bedford, MA, USA), and 1 ml of the filtered supernatant was mixed with 1 ml of phosphate-buffered saline (PBS, pH 7.2) and 10 mg of HPA. This mixture was incubated with shaking at 37°C for 2 h. After the reaction was terminated by adding 10% trichloroacetic acid, total protease activity was measured at 600 nm. ECP activity was normalized for each strain by dividing the total activity by OD_{600} value.

Western blot assay

For the immunoblotting assay, supernatants and bacterial cell pellets were harvested to the same OD_{600}. Then, 15 μl of each sample was loaded onto a 12% denaturing polyacrylamide gel; the proteins were resolved by electrophoresis and finally transferred to a PVDF membrane (Millipore, Bedford, MA, USA). The membranes were blocked

with a 10% skim milk powder solution and incubated with a Asp-, LuxR- (GL Peptide Ltd., Shanghai, China), Flag- or Myc-specific antiserum at a 1:2000 dilution (Sigma-Aldrich, St. Louis, MO, USA) and then incubated with horseradish peroxidase-conjugated goat anti-rabbit or anti-mouse IgG at a 1:2000 dilution (Santa Cruz Biotechnology, Santa Cruz, CA, USA). Finally, the blots were visualized with an ECL reagent (Thermo Fisher Scientific Inc., Waltham, MA USA).

Bacterial killing analysis

The bacterial killing analysis was performed as previously described (38). In brief, after the bacteria were cultured overnight, the density was adjusted to $OD_{600} = 0.5$, and then, the predator (*V. alginolyticus* strains) and prey cells (*E. coli*) were mixed at a ratio of 4:1. Then, 25 μl of this mixture were spotted on LBS agar plates and cocultured at 30°C for 4 h. CFU of the strains in the mixtures spotted on LBS agar plates at $t = 0$ were determined by plating 10-fold serial dilutions on appropriate plates. After 4 h, bacterial spots were collected from the LBS agar plates, and the CFUs of the surviving predator and prey were determined. An empty pBAD33 or pRK415 plasmid was used to render *E. coli* and *V. alginolyticus* resistant to chloramphenicol and tetracycline, respectively.

Infection of fish

All of the overnight cultured strains were harvested and then serially diluted with PBS. Zebrafish weighing approximately 0.25 g were infected with the strains at a dose of 10^5 CFU/fish via intramuscular (i.m.) injection according to a previous description (27). Zebrafish were anesthetized with tricaine methanesulfonate (MS-222) (Sigma-Aldrich) at a concentration of 80 mg/l. Thirty fish were infected with each dilution, and three parallel experiments were performed. Then, the fish death that was caused by vibriosis was recorded.

RESULTS

LuxR is a master QS regulator in *V. alginolyticus*

Three parallel autoinducer receptor systems are deployed in a *V. harveyi*-like QS system and culminate in the control of the production of LuxR, the TetR family transcription factor known as a MQSR (Figure 1A). In HCD, QS signal transduction induces LuxR production and thereby regulates the expression of virulence-associated genes. To characterize the cell density-dependent LuxR yield in *V. alginolyticus*, we introduced a P_{luxR}-*luxAB* reporter with the *luxR* promoter fused to *luxAB* gene into the wild-type (wt) strain. The *luxR* promoter activity was low at low cell density stage (~6E+8 CFU/ml, 2 h or LCD) as a result of AphA repression (18,27). Although a slight decrease in bioluminescence between 4 h to 8 h with an unknown mechanism, high *luxR* promoter activity was observed at high cell density (~6E+10 CFU/ml, 10 h or HCD) (Figure 1B). Then the *luxR* promoter activity was decreased after 10 h, probably due to the inhibition of LuxR to its own transcription (27). Similarly, analysis via qRT-PCR and Western blot assays with LuxR-specific antibody also showed low *luxR* transcription and expression levels at LCD and high levels at HCD (Figure 1C-D, and Supplementary Figure S1), indicating that LuxR expression is cell density-dependent.

We were intrigued how three parallel QS systems contribute to LuxR production and its downstream gene expression in *V. alginolyticus*. Single or combined deletion mutants for each of the autoinducer synthetases, i.e. *luxM* for AI-1, *luxS* for AI-2, and *cqsA* for CAI-1, were constructed (Supplementary Tables S1–2) and the expression of LuxR and Asp, a LuxR-controlled exotoxin (Supplementary Figure S1) (20), was determined. As previously established (24), the Δ*luxM* strains and Δ*cqsA* showed minimal Asp production while Δ*luxS* displayed slightly decreased Asp activity compared to the wt strain (Figure 1E-F). In line with the Asp production, LuxR production was undetectable in Δ*cqsA* and the Δ*luxM* strains and was slightly decreased in Δ*luxS*. The *luxM*, *cqsA* and *luxS* double and triple deletion mutants were abolished in LuxR production at all (Figure 1F). Taken together, these results indicated that the LuxM/N and CqsA/S systems are essential for LuxR and QS gene expression, while the LuxS/LuxPQ system may be partially involved in the expression of LuxR and genes downstream from LuxR.

Genome-wide identification of the LuxR regulon and binding sites

Transcriptomics analysis of the wt and Δ*luxR* strains indicated that a total of 168 genes were upregulated and 112 genes were downregulated in Δ*luxR* compared to the wt strain ($|\log_2 FC| \geq 1$-fold, $P_{adj} < 0.05$) (Figure 2A, and Supplementary Figure S2, Supplementary Tables S3–S4), indicating that LuxR serves as both a repressor and activator in *V. alginolyticus*. We performed chromatin immunoprecipitation and nucleotide sequencing (ChIP-seq) to determine the LuxR regulon (Supplementary Table S5). Because the sizes of the DNA fragments analyzed by ChIP-seq assays (~200 bp) are much larger than the LuxR homolog binding consensus sequences (16–28 bp) (8–10), the respective ChIP samples were subjected to DNase I-seq, i.e. DNA fragmentation, DNase I digestion, and nucleotide sequencing of the LuxR protected fragments (~50 bp), thus allowing mapping with higher resolution of LuxR binding sites (Supplementary Table S6). We used the Δ*luxR* strain harboring vector expressing Flag-tagged LuxR in ChIP assays with a strain expressing Flag alone as a negative control. Flag-LuxR behaved similarly to the wt LuxR, as Asp activity in Δ*luxR* was fully restored by introducing the vector expressing Flag-LuxR (Supplementary Figure S3A and B), thus validating the following ChIP- associated analysis.

The independent ChIP-seq assays and subsequent DNase I-seq analysis enabled mapping of the LuxR binding sequences to the *V. alginolyticus* genome. We identified 297 enriched loci harboring LuxR-binding peaks (enriched > 2-fold compared with the control sample) by ChIP-seq (Supplementary Table S5) and 101 enriched loci by DNase I-seq (enriched > 2-fold) (Supplementary Table S6), respectively. Moreover, 76 enriched loci revealed by DNase I-seq were overlapped with those identified by ChIP-seq (Figure 2A).

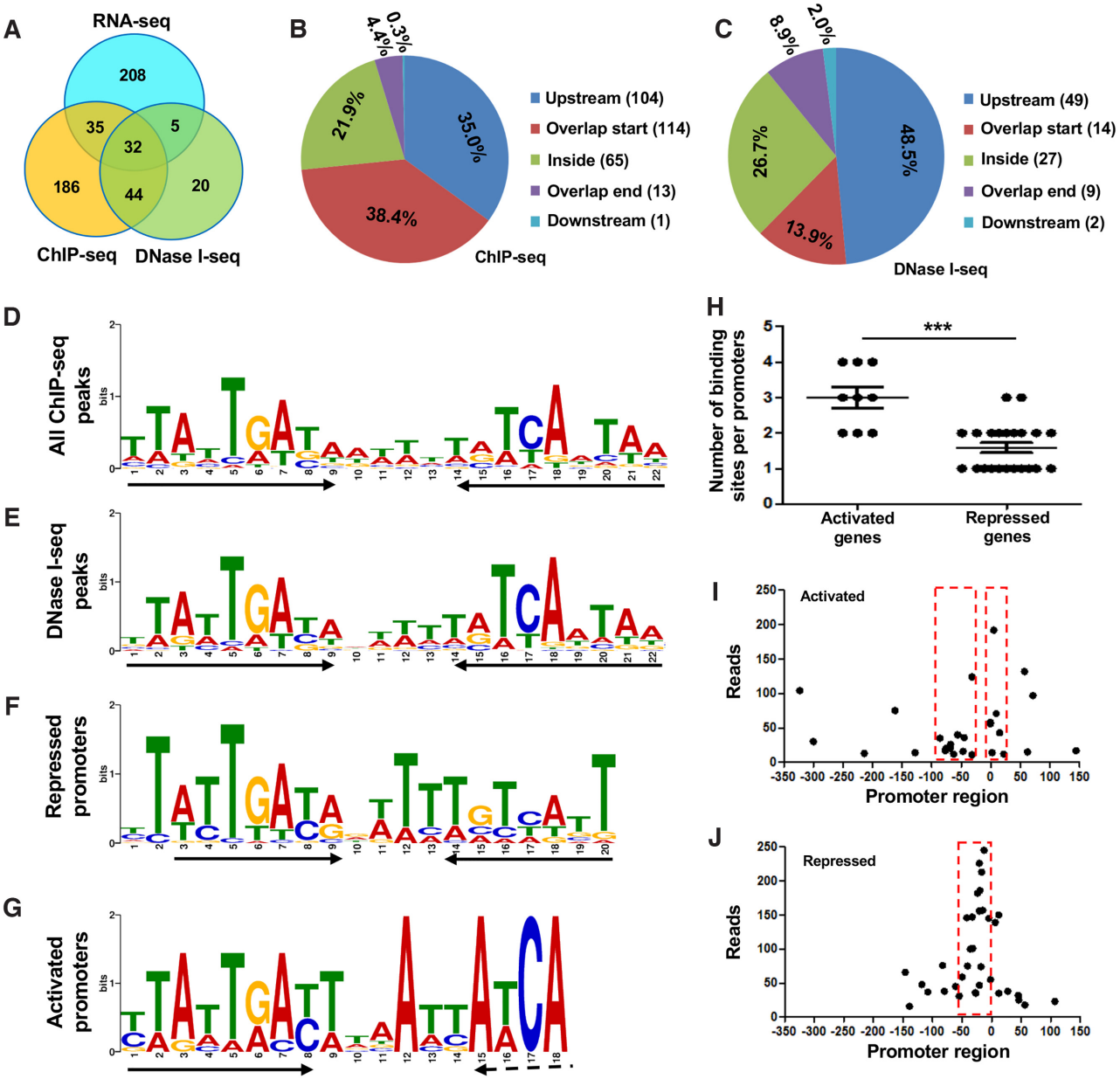

Figure 2. Genome-wide analysis of LuxR-binding sites in genes activated or repressed by LuxR. (**A**) Venn diagrams indicate the number of genes regulated by LuxR through RNA-seq, ChIP-seq, and DNase I-seq. (**B**, **C**) Pie chart of LuxR binding peak locations in various genes as revealed by ChIP-seq (B) and DNase I-seq (C). (**D–G**) LuxR binding motifs derived from MEME analysis of the ChIP-seq and DNase I-seq peaks under 'strand only' search mode. The binding motifs of all peaks from the ChIP-seq (D) and DNase I-seq (E) analyses, enriched peaks in the repressed promoters (F) and the activated promoters (G) are shown. Arrowed lines denote the complete (solid) or incomplete (dashed) inverted repeat relative to the left half part. (**H**) The number of binding sites in the LuxR repressed and activated genes, respectively. ***$P < 0.001$ (Student's t-test). (**I**, **J**) The normalized DNase I-seq reads of LuxR-binding sites in the subregions in activated (I) or repressed (J) promoters controlled by LuxR. The dashed boxes indicate the subregions containing a high density of LuxR binding sites.

These loci were located across the genome, including in intergenic regions and coding regions (Figure 2B and C, Supplementary Figure S4A–C). Based on the DNase I-seq data, peaks covering ∼30–50 bp sequences were identified in the strain expressing LuxR-Flag but not in the strain producing Flag alone. Validating the DNase I-seq analysis, the binding sites of LuxR protein at *luxR* promoter were consistent with those identified with the previous DNase I footprinting analysis (27).

Analysis with the MEME (multiple EM for motif elicitation) algorithm under the 'strand only' search mode revealed a 22-bp binding motif (5′-TTATTGATAAATTTATCAATAA-3′) showing sequence palindrome in the LuxR-binding sequences investigated by ChIP-seq (Figure 2D) and a 22-bp highly consistent sequence (5′-TTATTGATANTTTTATCAATAA-3′) detected by DNase I-seq (Figure 2E). These analyses showed an overall 9–4-9′ LuxR binding motif with 9-mer consensus palindrome sequence and

4-mer spacer sequence of low conservativeness. Highly similar logos were also generated with the same datasets under default or 'palindrome only' search mode (Supplementary Figure S4D–G).

Further analysis by RNA-seq and DNase I-seq showed that 37 enriched peaks were associated with LuxR-regulated genes (Figure 2A, Supplementary Table S6). We then separately analyzed the LuxR-enriched peaks in activated promoters ($n = 9$) and repressed promoters ($n = 22$). MEME analysis with various parameters, i.e. 'strand only', 'palindrome only' or default search mode, showed that the 20- or 21-bp LuxR-binding motifs in the repressed promoters had nearly palindromic sequence (Figure 2F and Supplementary Figure S4H and I), whereas the 18-bp LuxR-enriched motifs in the activated promoters had an incomplete inverted 9-mer repeat 'TTATTGATA' (Figure 2G and Supplementary Figure S4J). Notably, MEME analysis with 'palindrome only' parameter could not yield a significant (E-value < 0.05) logo from the enriched promoters of activated genes. The logos from these repressed and activated promoters were highly consistent with the motifs found in the *luxR* promoter region as revealed by the DNase I footprinting assay (27).

Moreover, the median number of LuxR binding sites for activated genes was 3 while that for repressed genes was 1.6 (Figure 2H), respectively, indicating that the binding site distribution patterns associated with the LuxR-activated and LuxR-repressed genes were significantly different ($P < 0.001$). The normalized reads for the LuxR-bound repressed promoters were higher than those for the activated promoter sequences (Figure 2I and J), suggesting a LuxR binding model with stronger binding affinity for repressed promoter sequence than for activated sequence. In addition, the peaks for activated genes were located at approximately –35 to –100 bp and 0 to +25 (Figure 2I), while those for the inhibited genes were located at 0 to –50 bp (Figure 2J). Taken together, more precise LuxR-binding sites were unraveled by ChIP-seq and DNase I-seq assays, which demonstrated totally distinct LuxR binding patterns for activated and repressed genes.

Validation of LuxR-mediated gene regulation

To validate the ChIP-seq and DNase I-seq data, four promoter regions of LuxR-targeted genes (RS20535, RS11155, *ppkA2* and *hcp2*) (Figure 3A, E, I, M) were selected for qRT-PCR analysis and electrophoretic mobility shift assays (EMSA). In a strain lacking *luxR* (Δ*luxR*), the transcripts of RS20535 and RS11155 were significantly upregulated, while those of *ppkA2* and *hcp2* were significantly downregulated, and the reintroduction of *luxR* into the strain restored the respective gene transcriptional levels to those of the wt strain, confirming the roles of LuxR in control of these genes (Figure 3B, F, J, N). In addition, retardation was also observed in the EMSAs with LuxR and the DNA probes harboring the respective promoter sequences in a concentration-dependent manner, indicating that LuxR protein can bind to all four promoters (Figure 3C, G, K, O). To further confirm the binding motif in the promoter of LuxR-repressed or LuxR-activated genes, we performed DNase I footprinting for each of the four promoters with purified LuxR protein. As expected, the results showed that LuxR protein protected 5′-TACGGTAATGACAAA TCGATCAGTAA-3′ (the underlined nucleotides indicate highly conserved sequences in the repDNA logo identified with DNase I-seq) in the promoter region of RS20535, and 5′-CCATAAATATGTGATTTATCAGTAA-3′ in the promoter region of RS11155 (Figure 3D, H). Similarly, LuxR fully or partially protected two distinct AT-rich sequences resembling the repDNA and actDNA binding motifs in the promoter of *ppkA2* and *hcp2* that were identified with DNase I footprinting analysis (Figure 3L, P), further underpinning lower DNA-binding affinity at these regions in the LuxR-activated genes as compared to those repressed genes revealed by DNase I-seq (Figure 2I and J) and EMSAs (Figure 3C, G, K, O). Taken together, these results confirmed the DNase I-seq and ChIP-seq data and the derived binding logos.

We further illuminated the genome-wide regulon of LuxR in *V. alginolyticus* (Supplementary Figure S5, Supplementary Table S3). Several functional categories of genes, including type II secretion system (T2SS), type VI secretion system 2 (T6SS2), cell motility and chemotaxis, two-component systems, pathogenesis-associated genes, metabolism pathways related to phosphotransferase systems, and the TCA cycle, were regulated by LuxR. In particular, previous investigations indicated that AphA, the LCD MQSR, and LuxR were essential for exotoxin Asp production and the bacterial virulence towards hosts (18,27). The promoter region of *asp* and *aphA* also carries a putative LuxR-binding motif. EMSA verified that LuxR binds the promoter region of *asp* and *aphA* (Supplementary Figure S6A and B). The increased level of LuxR led to a significant increase in Asp and a decrease in AphA (Supplementary Figure S6C and D), thus confirming that *asp* and *aphA* are included in the LuxR regulon. RNA-seq showed that all genes in the T6SS2 cluster were all downregulated in Δ*luxR* compared to their expression in the wt strain (Supplementary Figure S7A, Supplementary Table S3), and the promoters of the T6SS2 genes were enriched by LuxR in ChIP-seq and DNase I-seq assays (Supplementary Table S4). In addition, Western blot assays demonstrated that there was a strong reduction in *hcp2* expression in Δ*luxR* compared to the wt or Δ*luxO* strains (Supplementary Figure S7B). Moreover, interbacterial competition assays showed that Δ*luxR* lost the ability to kill *E. coli* (Supplementary Figure S7C), together with the finding that LuxR directly binds to the promoter regions of T6SS2 (Figure 3I-P, and Supplementary Figure S7A), further demonstrating that LuxR positively regulates the T6SS2 mediated bacterial killing function in *V. alginolyticus*. Taken together, the data show that LuxR is globally involved in the control of genes related to metabolism and virulence by binding to repDNA and actDNA to exert transcriptional regulation.

Overall structure of the LuxR-DNA complex

To understand the structural basis for DNA recognition by LuxR, we crystallized recombinant full-length LuxR in the presence of activation or repression double-stranded DNA. According to our *in vivo* DNase I-seq results, LuxR recognizes 22 DNA bases, but crystallization with a 22-mer

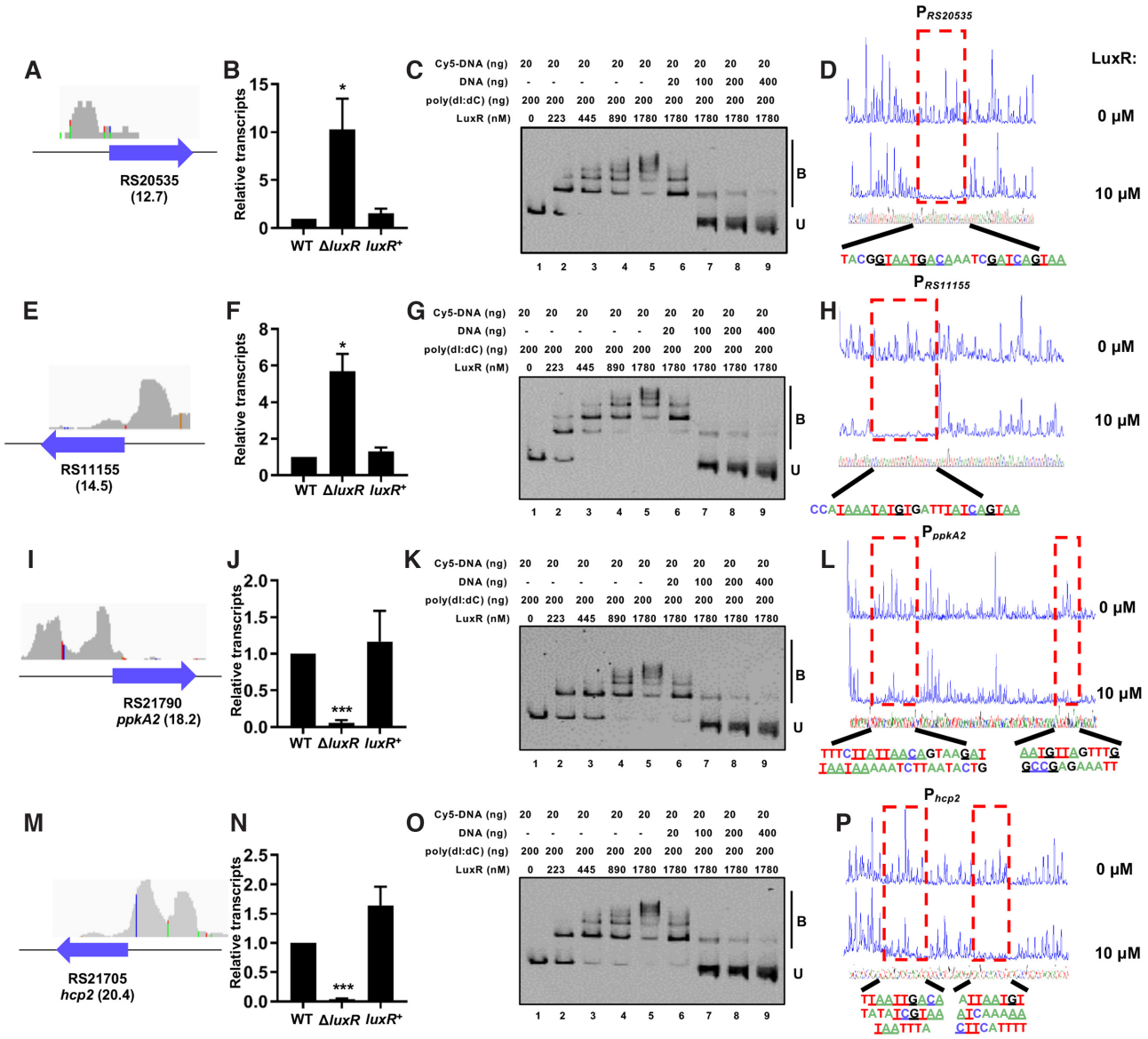

Figure 3. Verification of the LuxR-activated and LuxR-repressed genes by EMSA, qRT-PCR and DNase I footprinting analyses. (**A**–**P**) Verification of the ChIP-seq identification of LuxR-binding target genes RS20535 (A), RS11155 (E), *ppkA2* (I) and *hcp2* (M) by qRT-PCR (B, F, J, N), EMSA (C, G, K, O) and DNase I footprinting (D, H, L, P) analyses, respectively. The transcript levels of target genes in the WT, Δ*luxR* and *luxR*$^+$ strains were determined by qRT-PCR. $^*P < 0.05$, $^{***}P < 0.001$ (Student's *t*-test). An increasing amount of purified LuxR protein with the promoter regions was used for the EMSA and DNase I footprinting assay. The poly(dI:dC) was used as a non-specific competitor DNA, and the unlabeled DNA was used to compete the Cy5-labeled DNA. B, bound DNA; U, unbound DNA.

failed due to low diffraction quality. We resort to use an activation 21-mer DNA containing the LuxR-binding site I (LBSI or RBS3) from the *luxR* promoter (actDNA: 5′-ATAATGACATTACTGTATATA-3′), established by DNase I footprinting analysis (27) and DNase I-seq (Supplementary Figure S8C), and a 21-mer repression DNA containing the whole logo sequence (repDNA: 5′-TTATTGATAAAATTATCAATA-3′) (note that A4 and C8 were modified to T4 and T8, respectively, as they show the same frequency bits) (Supplementary Figure S4H) for the LuxR-DNA crystallization and structural analysis. We resolved the crystal structures of LuxR in complex with the actDNA and repDNA at 2.6 and 2.3 Å respectively (Table 1). In the crystal lattice of the LuxR-repDNA structure, Arg11 of subunit A binds the T-A base pair of the adjacent DNA duplex in the pseudofilament (Supplementary Figure S9).

Similar to the TetR-DNA complex, which was the first well-characterized member of the TetR-family transcriptional regulators (Figure 4A), both crystal structures of LuxR in complex with actDNA or repDNA, display one homodimer in the asymmetric unit, arranged as subunits A and B, which interacts with a double-stranded DNA via two conserved N-terminal DNA-binding domain (DBD). Each subunit of the LuxR homodimer displays two alpha helical domains with a similar fold to that of SmcR and HapR structures, which are the LuxR orthologs in *V. vulnificus* and

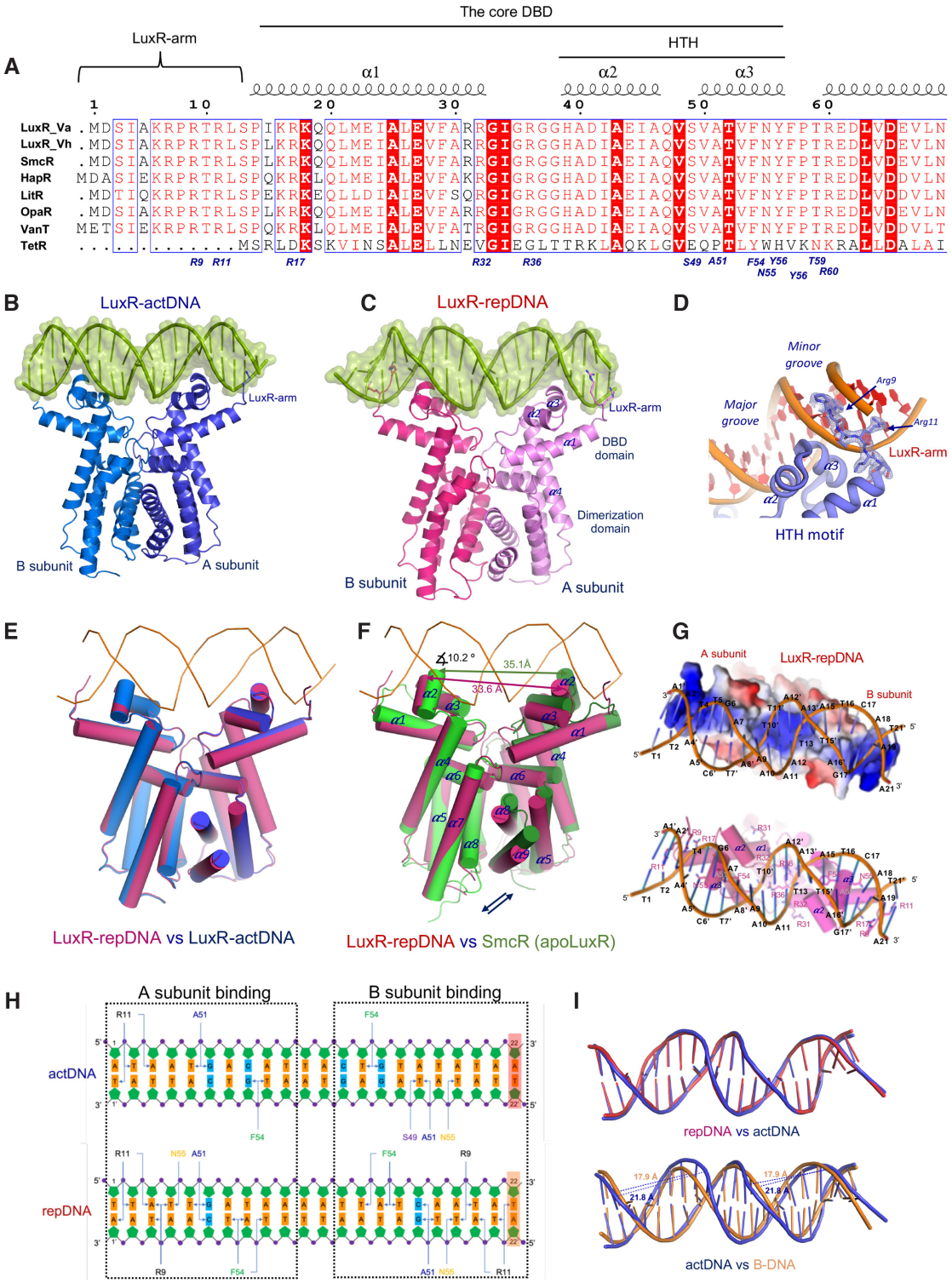

Figure 4. Structure of the LuxR-DNA complex. (**A**) Sequence alignment of TetR with LuxR family members in *V. alginolyticus* (LuxR_Va), *V. harveyi* (LuxR_Vh), *V. vulnificus* (SmcR), *V. cholerae* (HapR), *V. fischeri* (LitR), *V. parahaemolyticus* (OpaR) and *V. anguillarum* (VanT), labeling with the N-terminal extension (LuxR-arm), HTH motif and core DNA-binding domain (DBD). Residues involved in the interactions with DNA bases are marked. (**B**, **C**) Structures of the LuxR homodimer bound to an actDNA 21-mer (B) and repDNA 21-mer (C) are displayed. (**D**) Close-up view of the LuxR-arm interaction with the DNA minor groove in the LuxR-repDNA structure. Arg9 and Arg11 are shown with a 2*Fo* – *Fc* electron density map. (**E**, **F**) Structural superposition between LuxR-repDNA (magenta) with LuxR-actDNA (blue), and LuxR-repDNA (red) with SmcR (green). (**G**) Mixed surface and ribbon representation of LuxR-repDNA shows the highly positively charged DNA-binding surface. (**H**) Schematic representations of LuxR-actDNA and LuxR-repDNA contacts. Only interactions with <4 Å separating the amino acid residues from the bases of the cognate DNA are indicated by arrows for simplicity. The 22th T-A base pair from the adjacent DNA duplex in the pseudo-filament is marked. (**I**) Ribbon display of the superpositions of repDNA (magenta) and actDNA (blue) and of repDNA (magenta) and B-DNA (orange). The distances of the major grooves are indicated with dashed lines.

V. cholerae (5,6), containing the canonical helix-turn-helix motif (HTH), followed by a large α-helix C-terminal domain responsible for dimerization (Figure 4B and C). The overall structure of each subunit in the LuxR homodimer is very similar, with root mean square deviation (rmsd) values of 0.23 and 0.38 Å for the A and B subunits of LuxR-repDNA and LuxR-actDNA, respectively. Additionally, the structural comparison of the actDNA and repDNA LuxR homodimers with a rmsd value of 0.256Å (Supplementary Figure S10A), revealed that the bound DNA fragments consist of a distorted B-DNA double helix (rmsd of 0.744 Å), indicating a similar mode of interaction for both LuxR complexes (Figure 4E, I). Alignment with an ideal B-DNA revealed notable alterations in the regular double helix geometry, specifically in the two major grooves that interact with LuxR. Notably, the size differed from 17.9 Å for a standard B-DNA to 21.8 Å for the B-DNA in actDNA and repDNA bound to LuxR (Figure 4I).

LuxR contains a 12-residue N-terminal extension that precedes the core DBD, herein termed LuxR-arm, which is quite conserved in all LuxR homologs but is absent in TetR and many of other TetR family proteins (Figure 4A). In the crystal structures of apo SmcR and HapR, the conserved LuxR-arm is partially displayed and disordered. Although LuxR and TetR DBDs display a similar mode of binding to the DNA major groove through the HTH motif (rmsd of 0.440 Å), the LuxR-arm extension establishes an unexpected interaction with the DNA minor groove through Arg9 (R9) and Arg11 (R11) (Figure 4B-D). Arg9 and Arg11 are fully conserved in LuxR-Vh, SmcR, HapR and LitR, and probably play a similar role in these LuxR-type transcription factors (Figure 4A). This N-terminal extension is not found in other TetR transcription factor members, namely, DesT, TetR, CgmR, RcsB and QacR, for which protein-DNA structures are available (39–43).

LuxR shares low sequence identify with TetR, but approximately 73% and 92% identity with HapR and SmcR, respectively (44). Since the apo structure of LuxR is not available, this high sequence similarity allows us to compare the structures of apo SmcR with that of the LuxR-DNA complex to analyze the structural changes upon binding to DNA. Superimposition of one subunit of the apo-SmcR to holo-LuxR displayed rmsd values of 1.759, 1.402 and 0.643 Å for the whole molecule, the C-terminal dimerization/regulatory domain (residues 60–199), and the N-terminal DBD domains (residues 9–59), respectively, indicating a similar fold (Figure 4F and Supplementary Figure S10B).

LuxR dimer interface rearrangement

Alignment of one subunit in the homodimer of LuxR-DNA and SmcR (apo LuxR) causes a notable rigid-body displacement in other subunits, including important conformational changes in the homodimer interface (Figure 4E and F). DNA binding triggers a shift of ∼1.5 Å and a torsion of 10.2° between the two HTH motifs of the DBD domains (using the Cα of Ala51 as a reference point) to enable the protein to fit in the DNA duplex (Figure 4F). This fitting of the two N-terminal DBD domains into the DNA grooves produces a displacement at the dimer interface, resulting in important loop rearrangements and the creation of novel interface contacts (Supplementary Figure S10B–D). It is particularly interesting to observe residue rearrangements around the hinge region between the two DBDs, where the Arg32, Arg36 (from the α1–α2 loop) and Arg60 interaction with the phosphate backbone in the central minor groove induces important changes in the adjacent residues at the dimer interface (Supplementary Figure S10A-B). For example, DNA binding triggers the formation of an electrostatic interaction among Arg60–Glu124–Arg122–Glu116, which is not present in the apo form, with Arg122 playing the central role in this novel interface contact. Additionally, it is quite remarkable that, upon displacement by ∼5 Å, Glu124 interacts with Arg60 and that the novel hydrophobic pocket around Trp128 (Supplementary Figure S10C-D) is completely different from that of the apo LuxR structure.

Overall DNA recognition by LuxR

In both LuxR-actDNA and LuxR-repDNA structures, the subunit A is bound to the left half-site of the palindrome, whereas the subunit B binds to the right half-site of the palindrome (Figure 5A and B). The DBD of LuxR binds the major and minor DNA grooves through the HTH motif and LuxR-arm, respectively, forming extensive interactions with phosphates and bases in actDNA and repDNA (Figure 4G and H). The DNA-binding surface of LuxR is highly positively charged, thus displaying extensive contacts with the negative backbone phosphates, particularly in the three minor grooves formed by the DNA structure (Figure 4G). The most important difference between the LuxR-actDNA and LuxR-repDNA structures corresponds to the unique interaction of LuxR-arm with the two external minor grooves of the repDNA structure (Figure 4B and C).

LuxR-DNA backbone interactions

In both structures, the DNA phosphate backbones of the actDNA and repDNA sequences establish extensive polar interactions (including hydrogen bonds) in their major and minor grooves with Arg17, Arg32, Arg36, Ser49, Thr52, Tyr56, Pro58, Thr59 and Arg60 (Figure 5A and B). Among these interactions, the interactions between the guanidinium-positive groups of Arg32 and Arg36 with the phosphate DNA groups of the nucleotides at positions 13 and 14 (and the equivalent positions, 9′ and 10′, in the complementary DNA strand) are particularly relevant. These contacts are produced after a notable rearrangement of the α1–α2 loop that allows the interaction with the minor central groove and corresponds to a spacer in the middle of the palindromic DNA sequence, as observed by comparison with the apo LuxR (SmcR structure) (Supplementary Figure S10B).

Other backbone contacts include the interaction of the side chains of Arg17 and Tyr56 with the backbone phosphates of DNA nucleotides at positions 4 and 19′ in each complex, respectively. The main and side chains of Pro58, Thr59 and Arg60, located in the loop between helices α3 and α4, interact with the backbone phosphates at positions 14 and 15 (8′ and 9′ in the complementary DNA strand). The side chains of Ser49 and Thr55, located in the α3 of

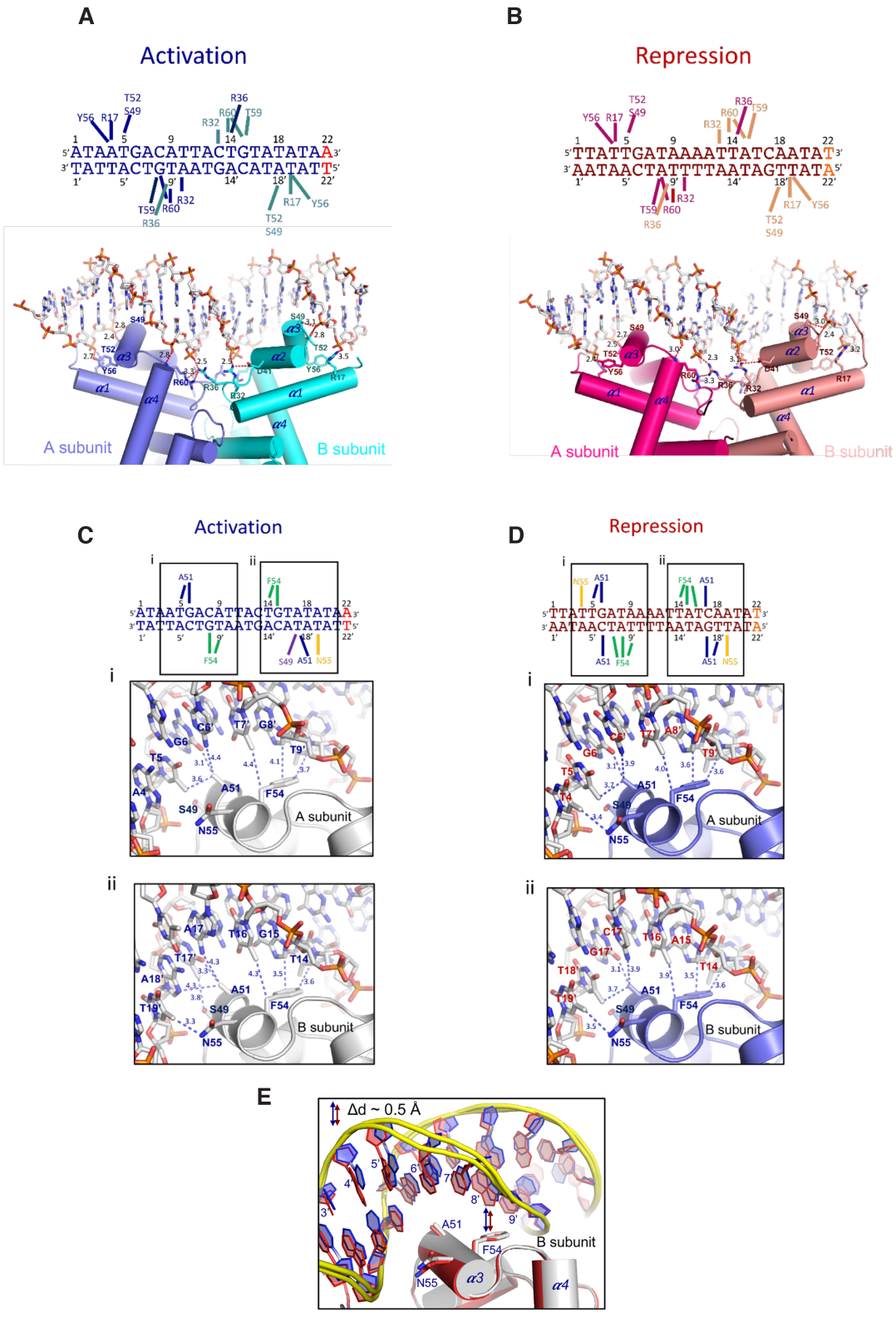

Figure 5. Interactions between the HTH motif and the DNA major groove. (**A–D**) Interactions between amino acid residues with phosphate backbone or DNA bases in actDNA (A and C) and repDNA (B and D) are represented by short lines and ribbon display. The colors of the interaction lines indicate the corresponding subunits. The detailed interactions between major groove bases and the HTH motif are shown in C-i and C-ii for actDNA, and in D-i and D-ii for repDNA. (**E**) Structural superposition shows that the repDNA (red) has the overall closer contact distances with LuxR than the actDNA (blue) has with LuxR.

the HTH motif of the major groove, are in close proximity to the phosphate backbone at position 5 (or 18′ in the other strand). Although LuxR establishes basically similar contacts through the backbone phosphates with both the repression and activation DNA sequences, the LuxR–repDNA complex displays globally closer contact distances than the LuxR-actDNA complex, probably reflecting a strong binding affinity (Figure 5A and B).

LuxR-DNA nucleobase interactions at the major groove

Normally, an analysis of specific contacts between the DNA nucleobases and LuxR would be essential to establish the structural basis for the different transcription activities between the actDNA and repDNA sequences. Nucleobase contacts in the major groove are realized by side chains of the residues emanating from α3 of the HTH motif in the DBD domain, namely Ser49, Ala51, Phe54 and Asn55 (Figure 5C and D). Ser49 only contacts T17′ in the B subunit of the activation complex, due to the unique presence of a thymine. Ala51 establishes close contacts with T5, G6 and C6′ (G17′, T18′ and C17 in the complementary strand) in the repression complex ((Figure 5C, i and ii). However, in the activation complex, due to the semipalindromic DNA sequence, some of these contacts are not established (Figure 5C ii), partly because of the adenine at position 18′.

Phe54 establishes an extensive van der Waals and hydrophobic contacts with T14, A15 and T16 nucleobases (T7′, A8′ and T9′ in the complementary DNA) in the repression complex (Figure 5D, i, ii). However, in the activation complex, only contacts with G14 and T15 (G8′ and T9′ in complementary DNA) are maintained (Figure 5C, i, ii). Finally, the side chain of Ans55 is within van der Waals distance of atom C7 in the methyl group of T4 (T19′) in the repression complex, which differs from the activation complex, in which this interaction is maintained only in subunit B (T19′), since position 4 in subunit A is occupied by adenine. Similar to the phosphate backbone interactions, the distances of the nucleobases to LuxR residues in the major groove are shorter in the repression complex, displaying an average distance difference of 0.5 Å in comparison to the activation complex (Figure 5E), further suggesting a stronger binding affinity of LuxR for the repDNA palindromic sequence.

LuxR-arm interaction with the minor groove

The major difference between LuxR-actDNA and LuxR-repDNA structures is revealed by the extensive contact interface displayed between the N-terminal extension LuxR-arm domain, mainly composed of Arg9 and Arg11, and the nucleobases of the two minor grooves in the repression complex (Figure 6A, D). In the activation complex, only Arg11 in the subunit A is observed to be in contact with one end of the semipalindromic DNA sequence (Figure 6B and C). However, in the LuxR-repDNA complex, both of the subunits establish extensive contacts with the minor groove through Arg9 and Arg11 (Figure 6E–H). In the LuxR-arm extension of the subunit A, Arg9 forms H-bond interactions with the nucleobases of T4 and T3′ and with the sugar phosphate backbone of T4, T5 and A2′ (Figure 6E), and Arg11 also forms H-bond interactions with the nucleobases and sugar phosphate backbones of T2, A3 and A1′ (or T1′ for actDNA) (Figure 6B, E). Since the repDNA sequence is palindromic, the LuxR-arm extension of the subunit B establishes equivalent contacts with nucleobases and sugar phosphate backbones, specifically with T20, A21, T18′ and T19′ for Arg9 and with T22, A20′ and T21′ for Arg11 (Figure 6G and H). Notably, position 22 is occupied by a thymine, not an adenine, as would be the case for a palindrome, because it is from the symmetric crystal neighbor; however, it displays a similar H-bond pattern as adenine. Finally, in contrast to the repression complex, in the LuxR-actDNA structure only the side chain of Arg11 in the subunit A forms H-bond interactions with the O2 atoms in the nucleobases of T2 and T1′, as well as H-bond interactions with the O4′ atoms in the sugar phosphate backbone of T2 and A3 (Figure 6B and C).

The major difference between the activation and repression DNA sequences in the LuxR-arm interaction is revealed at positions 1′ and 4, which may be either a thymine or adenine. Whereas both nucleobases in position 1′ can establish equivalent H-bond interactions with Arg11, as shown in our structures (Figure 6A, D), it is possible that the presence of adenine in position 4 might play a role in the decrease in the affinity of the sequence for LuxR in the activation complex.

In vitro validation of DNA recognition by the LuxR-arm domain

Our structures revealed the DNA recognition by the LuxR-arm domain. To determine how the interaction affects DNA-binding affinity, we performed EMSA experiments with wt or variant LuxR proteins and various DNA probes. First, we investigated the contribution of the full-length LuxR-arm and the LuxR-arm with mutated R9/R11 residues to LuxR-arm binding with actDNA (Figure 7A and Supplementary Figure S11) and repDNA (Figure 7B and Supplementary Figure S11). Compared to wt LuxR (K_d = 449 nM for actDNA) and the LuxR variant with a residue substitution K16A not related to DNA binding (K_d = 329 nM), the R11A and R9/11A mutants ($LuxR^{R11A}$ and $LuxR^{R9/11A}$) as well as a variant with the LuxR-arm domain deleted in LuxR ($LuxR^{\Delta LuxR\text{-}arm}$) were unable to bind with actDNA, except for $LuxR^{R9A}$ which showed significantly decreased binding affinity for actDNA (K_d = 698 nM), which is consistent with the observation that R11 of LuxR is the essential residue for the minor groove interaction in the LuxR–actDNA structure (Figure 6A). Although the involvement of R9 in the LuxR–actDNA interaction was not observed, the residue is assumed to be involved in DNA binding in support of R11 inserting into the minor groove to interact with the specific nucleobases.

An overall higher affinity was observed for the LuxR-repDNA interaction as compared to the LuxR-actDNA interaction (Figure 7B and Supplementary Figure S11). Compared to wt LuxR (K_d = 157 nM for repDNA), the $LuxR^{R9A}$ and $LuxR^{R11A}$ variants exhibited severely decreased binding affinity for repDNA, with K_d values of 434 and 1057 nM, respectively (Figure 7B). Although a significant reduction was observed for repDNA affinity for $LuxR^{R9A}$, the R11A mutant was more close to LuxR-arm

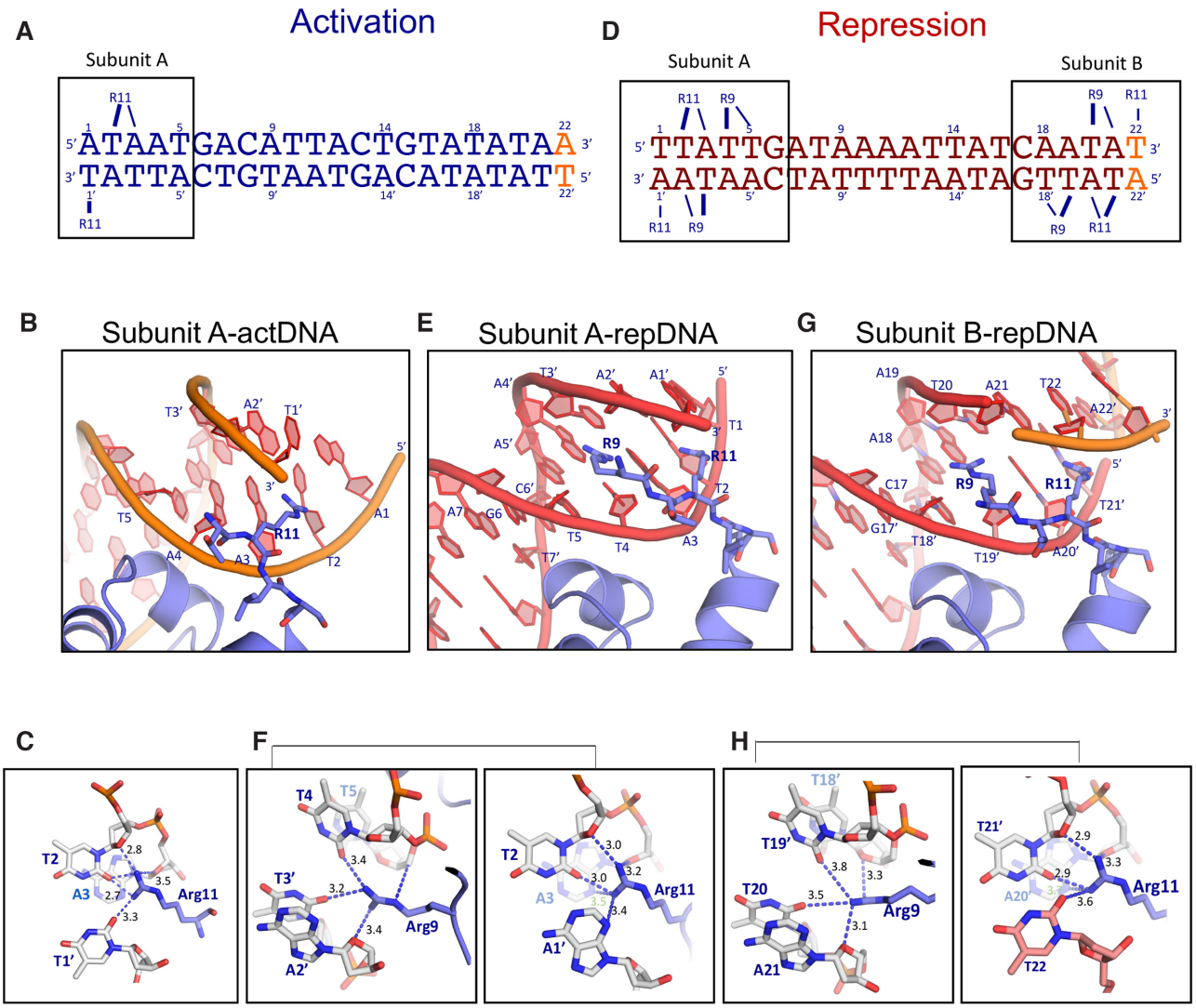

Figure 6. Interactions between the LuxR-arm and the DNA minor groove. (**A**, **D**) The interactions between amino acid residues and nucleotides in the minor grooves in actDNA (A) and repDNA (D) are shown by short lines. (**B**, **C**, **E**–**H**) The detailed interactions in the minor grooves are presented by ribbons and sticks in (B) and (C) for subunit A of LuxR-actDNA, and (E), (F) for subunit A, (G), (H) for subunit B of LuxR-repDNA.

deletion and R9/11A-double mutant, resulting in drastically decreased DNA binding (Figure 7B). These data indicated that both R9 and R11 residues of LuxR are essential for the LuxR-repDNA recognition, although R11 mediates a stronger interaction than R9 (Figure 7B). Intriguingly, the $LuxR^{\Delta LuxR\text{-}arm}$ showed residual but extremely low (i.e. the K_d could not be calculated (ND)) affinity to repDNA as compared to the mutant with R9/R11A double substitutions, suggesting that the presence of a flexible N-terminal extension that cannot interact with the minor groove at all (R9/R11A) might perturb or hinder the major groove binding by the DBD domain in the $LuxR^{R9/11A}$ variant.

We also carried out *in vitro* assays to validate the contribution of key nucleobases mediating actDNA or repDNA recognition by LuxR (Figure 7C, D and Supplementary Figure S11A). In comparison to the wt actDNA ($K_d = 449$ nM), only the substitutions at T2A (AM1) and A3C (AM7), which abolish the observed R11 interaction, caused reduced binding affinities ($K_d = 1686$ nM for AM1and $K_d = 636$ nM for AM7) for LuxR (Figure 7C). Nevertheless, the mutant containing the substitution of A4T (AM6) resulted in the increased affinity for LuxR, which might be due to the creation of interactions of R9 in subunit A, as shown in the LuxR-repDNA structure (Figure 6A). Similarly, the multiplex substitutions, i.e. A1T, A4T and A22T in actDNA (AM5), also resulted in the increase in affinity for LuxR (Figure 7C). The other single or multiplex mutant containing T18A (AM2–4) in actDNA did not seem to significantly affect the binding affinity, which might be due to the generation of possible interactions for R9 or R11 and disruption of the HTH mediated DNA-protein interactions (Figures 6A and 7C). As expected, the T22G (RM1), A21G (RM2), T20G (RM3), T2G (RM4) and A18T (RM5 and RM6) mutations that eliminated the interactions of the mutants at R9 and R11 residues showed a significant reduction in the binding affinity of LuxR-repDNA and verified that these nucleobases mediate key interactions during repDNA binding with LuxR. The multiplexed mutations of T1A, T4A

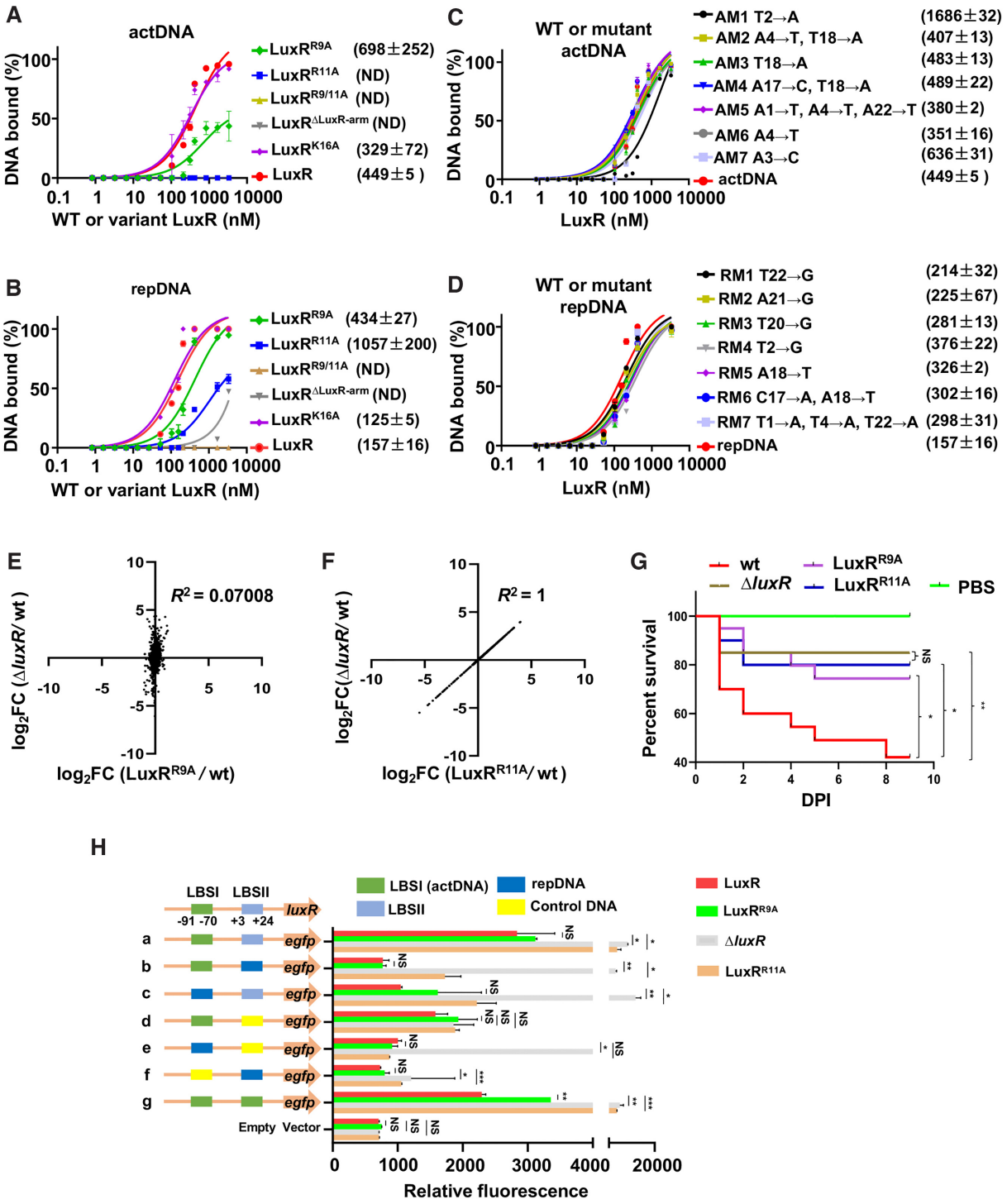

Figure 7. The residues Arg9 (R9) and Arg11 (R11) in the LuxR-arm domain are essential for LuxR-DNA interactions and QS regulation. (**A**, **B**) DNA binding of wt and variants of LuxR. DNA binding curves from the quantitative analysis of bound bands in EMSAs (see Supplementary Figure S11 for a representative example) are shown for $LuxR^{R9A}$, $LuxR^{R11A}$, $LuxR^{R9/11A}$, $LuxR^{\Delta LuxR\text{-}arm}$, $LuxR^{K16A}$ and LuxR with actDNA (A) and repDNA (B). (**C**, **D**) LuxR protein binding to the respective mutant actDNA (C) and repDNA (D) fragments (Supplementary Figure S11). The densitometric intensities of the bound DNA fragments were determined and plotted against the protein concentrations. Triplicate assays were performed. Dissociation constants (K_d, nM) are shown in brackets. ND, not detectable. (**E**, **F**) Scatter plots of gene expression in Δ*luxR* and the Δ*luxR* strains chromosomally expressing $LuxR^{R9A}$ (E) and $LuxR^{R11A}$ (F) relative to wt. (**G**) Survival analysis for zebrafish challenged with wt, Δ*luxR*, or the Δ*luxR* strains chromosomally expressing $LuxR^{R9A}$ or $LuxR^{R11A}$. The *P* values were calculated using a Kaplan–Meier survival analysis with a log-rank test. $^*P < 0.05$, $^{**}P < 0.01$. (**H**) Activities of P_{luxR} and its variants fused to *egfp*. P_{luxR} harbors two LuxR-binding sites, LBSI (actDNA, green) and LBSII (close to repDNA, light blue). The variant P_{luxR} was constructed with the substitutions of repDNA (blue) or 22-bp nonrelated control DNA (yellow). All promoter activities were assayed in the context of the Δ*luxR* or the Δ*luxR* strains chromosomally expressing wt LuxR, $LuxR^{R9A}$ or $LuxR^{R11}$ cultured for 9 h and the results were normalized by the activity of the wt strain. The results are presented as the means ± S.D. ($n = 3$). $^*P < 0.05$, $^{**}P < 0.001$, $^{***}P < 0.0001$ (Student's *t* test).

and T22A in RM7, which abrogates the R9 interaction and somewhat transforms the DNA residues into actDNA, also results in significantly reduced binding affinity of LuxR-repDNA (Figure 7D). Collectively, these data validated that R9 and R11 in LuxR-arm interactions with specific nucleobases play important roles in LuxR–DNA binding.

In vivo analysis of DNA recognition and QS gene regulation by the LuxR-arm domain

We characterized the QS regulation behavior of the LuxR variants in vibrios. The Δ*luxR* mutant stains chromosomally expressing wt or mutant forms of LuxR, ΔLuxR-arm, $LuxR^{R9A}$, $LuxR^{R11A}$, $LuxR^{R9/11A}$, $LuxR^{R9E}$, $LuxR^{R11E}$, were constructed and showed various levels of Asp production (Supplementary Figure S12). The significantly decreased Asp yields in the strain expressing R9 and R11 and the ΔLuxR-arm-related LuxR variants further demonstrated their essential roles in QS regulation (Supplementary Figure S12). Notably, the $LuxR^{R9E}$ strain exhibited a much lower level of Asp production than $LuxR^{R9A}$, probably due to the electric repulsion of the DNA interaction by the Glu substitution, demonstrating the important role of R9 in regulation of *asp* expression (Supplementary Figure S12). Comparative transcriptomic assays and ChIP-seq analysis facilitated the identification of the regulon by these LuxR proteins. The low level of consistency between $LuxR^{R9A}$-controlled genes ($R^2 = 0.07$) and genes affected by *luxR* deletion, compared with $LuxR^{R11A}$ and that of *luxR* deletion-regulated genes ($R^2 = 1$) (Figure 7E, F, Supplementary Figure S2), demonstrated that R11 is more important than R9 for LuxR function in QS regulation. Moreover, the $LuxR^{R11A}$ regulated considerably fewer of genes than $LuxR^{R9A}$ or wt LuxR as revealed by RNA-seq (Supplementary Figure S2E) and ChIP-seq (Supplementary Figure S13), confirming that R9 and R11 in the LuxR-arm play pivotal roles in DNA binding and transcriptional regulation.

Quorum sensing plays an important role in the pathogenesis of *V. alginolyticus* (27). We used zebrafish as a model system to test the effects of R9 and R11 in the LuxR-arm on the virulence of *V. alginolyticus* (Figure 7G). Groups of zebrafish ($n = 30$) were acclimated for at least 4 weeks before the infection experiments were performed with a dose of 10^5 CFU/fish. A significant difference ($P < 0.05$) in the survival rates was observed between the groups of fish treated with wt and Δ*luxR* strains, consistent with a previous observation (27). The survival of the fish in the groups treated with strains producing $LuxR^{R11A}$ or $LuxR^{R9A}$ was also significantly higher ($P < 0.001$) than that of those treated with wt, indicating that R9A and R11A mutants significantly attenuated the virulence of *V. alginolyticus* in fish. Taken together, vibrios seem to adopt a regulatory mechanism by using the N-terminal LuxR-arm domain for versatile gene modulation in *V. harveyi*-like QS cascades.

LuxR binding profiles and LuxR-arm domain coordinate QS output

Our DNase I-seq analysis and a previous investigation revealed two distinct LuxR-binding sites harboring the actDNA motif (LBSI, –91 to –70 bp) and a motif sequence resembling repDNA (LBSII, +3 to +24 bp), respectively, in the P_{luxR} region (Figure 7H). This finding represents a common profile of LuxR-binding sites in the promoter region of the LuxR-repressed or activated genes (Supplementary Figure S8). We substituted chromosomal LBSI or LBSII with the palindromic sequence (repDNA) used for the crystal structure determination and a nonrelated GC-rich 22-bp sequence that is not bound by LuxR as a control (Supplementary Figure S11B), to test their effect on P_{luxR} activities in the context of *V. alginolyticus* expressing wt or variant LuxR ($LuxR^{R9A}$, and $LuxR^{R11A}$). Except in the P_{luxR} strains with LBSI or LBSII sequences replaced with control DNA that appeared to totally destroy the P_{luxR} activity (Figure 7H, d and f), all the strains with *luxR* deleted (Δ*luxR*) showed high level of GFP fluorescence, indicating the overall repression of LuxR on P_{luxR} activity, consistent with the previous finding showing that LuxR acts as a repressor of *luxR* expression (27). Compared to the Δ*luxR* strain, the LuxR-producing strain reduced the wt P_{luxR} activity by 4.6-fold (Figure 7H, a). The repression effect of LuxR on the P_{luxR} variants (with LBSI or LBSII replaced by repDNA) (b, c, and e) was significantly increased, by 8.6-,12.9-, and 4.0-fold, respectively. Similarly, LuxR repression to P_{luxR} variants in which LBSII was replaced with actDNA (g) decreased to 3.6-fold, indicating the expected derepression activity mediated by actDNA. These analyses indicated that the LuxR-binding sequences and their relative positions in P_{luxR} together determine the extent of LuxR repression or activation at specific promoters. Moreover, $LuxR^{R9A}$ and $LuxR^{R11A}$ mutant proteins exhibited various degrees of attenuated repression, compared to that of wt LuxR in P_{luxR}, further demonstrating that the R9 and R11 in the LuxR-arm domain play key roles in regulating QS gene expression.

We also detected the overall much lower activities of P_{luxR} and its variants at LCD (2 h) (Supplementary Figure S14). The substitution of +3 to +24 bp repDNA sequence with the LBSI DNA in a strain producing LuxR also activated the *luxR* transcription as it did at HCD (Figure 7H and Supplementary Figure S14, a and g). In contrast, the replacement of LBSI sequence at –91–70 bp with repDNA significantly impaired the promoter activities in the LuxR generating strain at both LCD and HCD stages (Figure 7H and Supplementary Figure S14, a and c), demonstrating the potential activation function of LBSI in *luxR* transcription. Collectively, these analyses demonstrated that the features of LuxR-binding sequences, the profiles of the binding site position in the controlled promoters, and the R9/R11 recognition mode of the LuxR-arm domain enable the flexible control of gene expression and coordinate QS output in vibrios.

DISCUSSION

LuxR-mediated gene regulation is conserved among Vibrios

V. harveyi-type QS is common to most vibrios and represents the major model for QS studies for which TetR family LuxR homologs is known as MQSR to control the QS output (2). LuxR is unique as it cannot bind ligands and is distinct from TetR, as it acts as a global regulator with high

DNA binding flexibility to control the expression of hundreds of genes by both activation and repression activity, with the underlying mechanisms remaining unknown (4,8).

Many tiers of factors are assumed to govern the LuxR-centered QS output for various collective phenotypes, e.g. the upstream autoinducer signaling cascades of *luxR* expression, the DNA binding sites and their distribution in genes, and the manner by which LuxR interacts with specific DNA (45–48). Although further analysis of the signaling dynamics of the QS input is warranted, conserved QS components, such as LuxO, *qrr*s, and AphA, have been identified, demonstrating that *V. alginolyticus* harbors QS systems resembling that of *V. harveyi* (12,18,49). Here we also validated that LuxR behaves similarly in *V. alginolyticus* and *V. harveyi* because our RNA-seq and ChIP-seq analysis revealed a large group of overlapping genes (∼67) controlled by LuxR, including genes associated with T1/T3/T6SS, c-di-GMP signaling, flagellin, the ABC transporter system and QS genes, such as *luxR* (Supplementary Figure S5) (50). The gene encoding the *V. alginolyticus*-specific exotoxin Asp was revealed to be directly controlled by LuxR (Supplementary Figure S6), demonstrating the presence of a species-specific QS regulon in vibrios. Taken together, these analyses indicate that LuxR regulon is largely shared by *V. harveyi*-like QS systems, but the temporal variance in the regulons controlled by LuxR and QS remains to be elucidated.

Moreover, our ChIP-seq analysis coupled with DNase I-seq assays allowed us to dissect at a high-resolution LuxR-binding motifs i.e. actDNA and repDNA. In particular, the actDNA binding sequences generated logos with an asymmetric half right of the motif (Figure 2G). Both the actDNA and repDNA sequences are highly similar to that established for LuxR homologs in *V. harveyi* with ChIP-seq analysis (8), suggesting conserved regulatory mechanisms adopted by LuxR homologs in vibrios.

Distinct features of LuxR binding sites dictate gene activation and repression

DNase I-seq facilitated determination of the binding-site distribution profiles in the LuxR-targeted promoters. Multiple binding sites in a single LuxR-controlled promoter normally correlates with activation, but it is not always the case, as some exceptional LuxR-controlled promoters containing a mixture of both repDNA or actDNA binding sites in the otherwise activated or repressed promoters, e.g. the previous established P_{luxR} (Figure 7H and Supplementary Figure S8). This indicated that other levels of complexity, such as the presence of other DNA-binding proteins that modulate the binding complex (51), can affect LuxR-dependent genes' expression. However, our structural analysis and cellular assays using a single binding site appear to support a model in which the LuxR binding affinity is sufficient to determine activation or repression (Figure 7H, e).

The different binding affinities for the DNA sequence might determine the fate of polymerase activity, i.e., transcription or inhibition. Taking P_{luxR} as an example, LuxR represses transcription by binding to the positions of LBSII (close to repDNA) where RNAP binds or passes over. In this case, stronger binding affinity leads to greater repression (Figure 7H). The activation role of LuxR is accomplished by the recruitment of RNAP, which requires LuxR to bind to the upstream site of RNAP (LBSI, actDNA). In this case, the strong binding affinity of LuxR for LBSI positions would lead to repression since the strong binding affinity of LuxR for DNA arrests RNAP to prevent its release. Thus, our results support a mechanism for the master regulator LuxR with different binding affinities (strong or weak) that account either for repression, the RNA polymerase cannot displace LuxR from the binding site and transcription is repressed, or for activation, the RNA polymerase machinery goes through and transcribes the LuxR-dependent gene.

We thus proposed a model in which LuxR binds to the repDNA with high affinity at –50 bp to +1 bp for occlusion of RNAP binding at the promoter region and transcription initiation (Figure 8, bottom). In contrast, most of the LuxR-binding sites at an activated promoter are located from –30 bp to –100 bp relative to the transcriptional start site, indicating that LuxR can be classified as type I transcriptional factor (52) and facilitates the recruitment of RNAP as it interacts with the C-terminus of the α-subunit (51,53). The nearly doubled LuxR binding site number in the activated genes, the larger range of distribution in upstream or downstream of the promoter region and the lower affinity of LuxR for actDNA, as discussed below, may facilitate LuxR alterations of the chromosome conformation to recruit RNAP and trigger transcription initiation complex formation for gene expression (Figure 8, bottom).

Structural bases of unique DNA binding by LuxR

Crystal structures of the LuxR-DNA complex revealed a new mode of DNA binding by a TetR-family transcriptional regulator that involves a N-terminal extension binding to the minor groove. Compared to the LuxR–actDNA interaction, stronger binding affinity for the palindromic repression sequence is basically caused by both-end contacts involving the N-terminal LuxR-arm extension (Figure 8, up). In particular, Arg9 and Arg11 from both dimer subunits establish 18 H-bond contacts with nucleobases in the two minor grooves of the DNA double helix in the LuxR–repDNA complex. DNA recognition by the binding of Arg9 and Arg11 to nucleobases in the minor grooves is unique to the LuxR proteins in the TetR family. Other TetR family members also have a disordered N-terminal extension that mediates its binding in the DNA minor groove, such as SimR, in which Arg18 interacts with thymine in the minor groove, and Arg19 and Arg22 interact with phosphate backbones (54). However, the N-terminal extensions of LuxR and SimR are not conserved, and their modes of interaction with DNA minor groove are distinct. Moreover, LuxR can flexibly bind to the actDNA and repDNA with one end or both LuxR-arm structures, while SimR only binds to DNA using both of its N-terminal extensions, which renders the roles of LuxR and SimR in modulating DNA binding highly divergent. Notably, an adjacent C-terminal arm of TZAP 11th C2H2 zinc finger also recognizes the minor groove of telomeric DNA through the arginine-thymine pattern in eukaryotes (55).

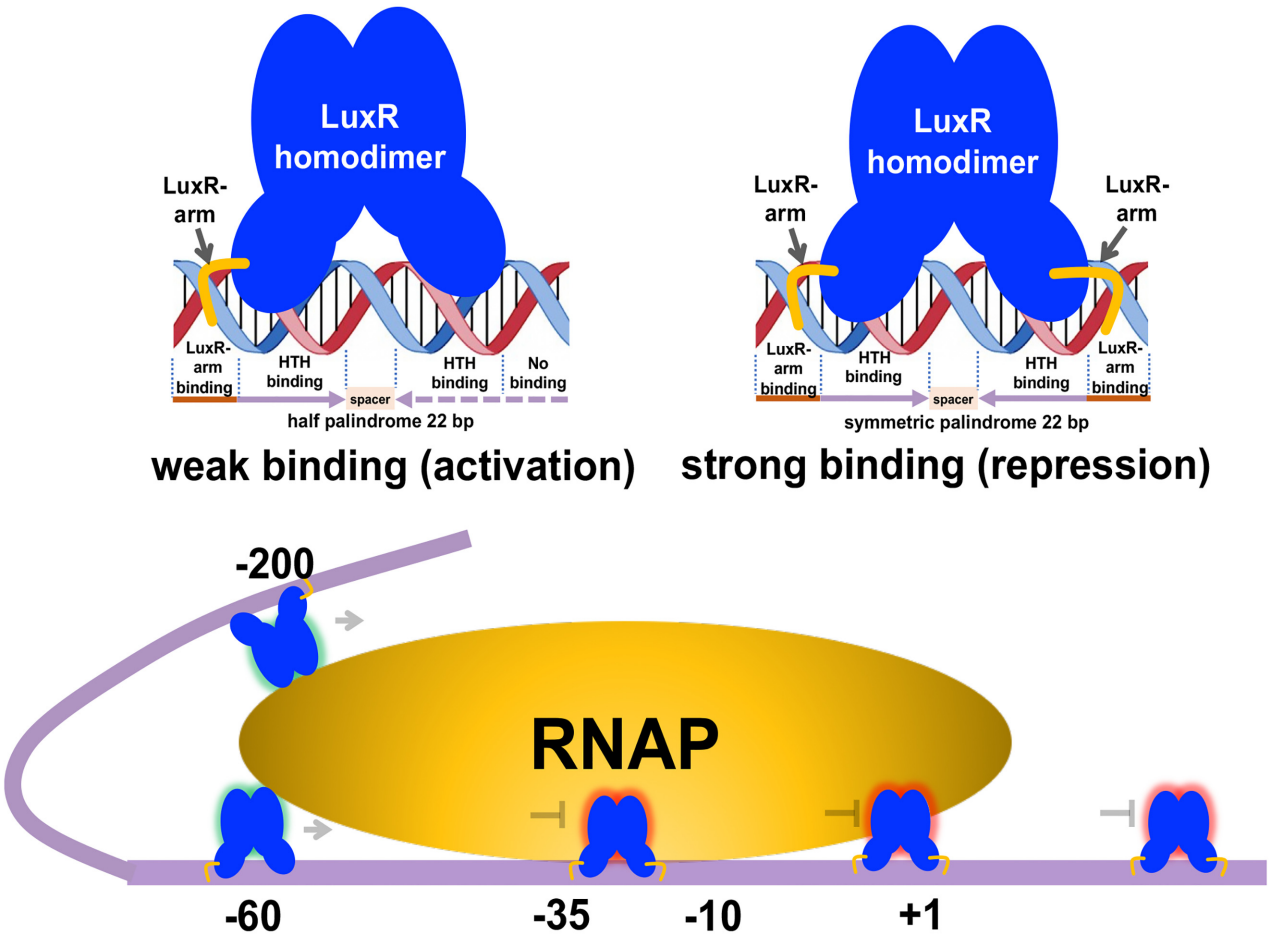

Figure 8. The working model of LuxR interaction with actDNA and repDNA and their binding patterns to control QS gene expression. The numbers indicate the location relative to transcription start site; arrows indicate transcription activation and bar-ended short lines show transcription repression (lower panel).

Finally, fundamental understanding of the LuxR mediated QS regulation in vibrios may facilitate to develop strategies, such as designing QS inhibiting chemicals that interfere with LuxR regulation to effectively control the pathogen threatening health to both humans and the aquatic animals. The knowledge of regulation machinery of the MQSR LuxR in vibrios also help to design promising genetic parts or circuits useful for the synthetic biology.

ETHICS STATEMENT

All animal protocols used in this study were approved by the Animal Care Committee of the East China University of Science and Technology (2006272). The Experimental Animal Care and Use Guidelines from Ministry of Science and Technology of China (MOST-2011-02) were strictly followed.

DATA DEPOSITION

The ChIP-seq, DNase I-seq and RNAS-seq sequence reads were deposited in the NCBI SRA database (PRJNA660595 and PRJNA673251). The accession numbers for LuxR-repDNA and LuxR-actDNA structures are 7AMN and 7AMT, respectively.

SUPPLEMENTARY DATA

Supplementary Data are available at NAR Online.

ACKNOWLEDGEMENTS

Author contributions: Conceptualization: W.Q.; Data curation: W.Q., R.D., Z.J., L.B., GD. Funding acquisition: W.Q., M.Y., R.D.; Investigation: Z.J., L.B., G.D., H.Y., C.M., M.Y., Z.X. Project administration: W.Q.. Supervision: W.Q. Validation: R.D., W.Q.. Visualization: W.Q., R.D. Writing – original draft: W.Q., R.D., Z.X., Z.J., L.B., G.D. Writing – review & editing: W.Q.

FUNDING

National Natural Science Foundation of China [31772891 to Q.W., 31772893 to Y.M.]; Ministry of Agriculture of China [CARS-47-G17]; Science and Technology Commission of Shanghai Municipality [17391902000]; Fundamental Research Funds for the Central Universities [22221062017019]; Ministerio de Ciencia, Innovación y Universidades [PGC2018-098423-B-I00 to D.R.]. Funding for open access charge: National Natural Science Foundation of China.

Conflict of interest statement. None declared.

REFERENCES

1. Papenfort,K. and Bassler,B.L. (2016) Quorum sensing signal-response systems in Gram-negative bacteria. *Nat. Rev. Microbiol.*, **14**, 576–588.
2. Henke,J.M. and Bassler,B.L. (2004) Three parallel quorum-sensing systems regulate gene expression in *Vibrio harveyi*. *J. Bacteriol.*, **186**, 6902–6914.
3. Plener,L., Lorenz,N., Reiger,M., Ramalho,T., Gerland,U. and Jung,K. (2015) The phosphorylation flow of the *Vibrio harveyi* quorum-sensing cascade determines levels of phenotypic heterogeneity in the population. *J. Bacteriol.*, **197**, 1747–1756.
4. Ball,A.S., Chaparian,R.R. and van Kessel,J.C. (2017) Quorum sensing gene regulation by LuxR/HapR master regulators in vibrios. *J. Bacteriol.*, **199**, e00105-17.
5. De Silva,R.S., Kovacikova,G., Lin,W., Taylor,R.K., Skorupski,K. and Kull,F.J. (2007) Crystal structure of the *Vibrio cholerae* quorum-sensing regulatory protein HapR. *J. Bacteriol.*, **189**, 5683–5691.
6. Kim,Y., Kim,B.S., Park,Y.J., Choi,W.C., Hwang,J., Kang,B.S., Oh,T.K., Choi,S.H. and Kim,M.H. (2010) Crystal structure of SmcR, a quorum-sensing master regulator of *Vibrio vulnificus*, provides insight into its regulation of transcription. *J. Biol. Chem.*, **285**, 14020–14030.
7. Ramos,J.L., Martínez-Bueno,M., Molina-Henares,A.J., Terán,W., Watanabe,K., Zhang,X., Gallegos,M.T., Brennan,R. and Tobes,R. (2005) The TetR family of transcriptional repressors. *Microbiol. Mol. Biol. Rev.*, **69**, 326–356.
8. Kessel,J.C., Ulrich,L.E., Zhulin,L.B. and Bassler,B.L. (2013) Analysis of activator and repressor functions reveals the requirements for transcriptional control by LuxR, the master regulator of quorum sensing in *Vibrio harveyi*. *mBio*, **4**, e00378-13.
9. Tsou,A.M., Cai,T., Liu,Z., Zhu,J. and Kulkarni,R.V. (2009) Regulatory targets of quorum sensing in *Vibrio cholerae*: evidence for two distinct HapR-binding motifs. *Nucleic Acids Res.*, **37**, 2747–2756.
10. Lee,D.H., Jeong,H.S., Jeong,H.G., Kim,K.M., Kim,H. and Choi,S.H. (2008) A consensus sequence for binding of SmcR, a *Vibrio vulnificus* LuxR homologue, and genome-wide identification of the SmcR regulon. *J. Biol. Chem.*, **283**, 23610–23618.
11. Jacobs Slifka,K.M., Newton,A.E. and Mahon,B.E. (2017) *Vibrio alginolyticus* infections in the USA, 1988–2012. *Epidemiol. Infect.*, **145**, 1491–1499.
12. Rui,H., Liu,Q., Wang,Q., Ma,Y., Liu,H., Shi,C. and Zhang,Y. (2009) Role of alkaline serine protease,*asp*, in *Vibrio alginolyticus* virulence and regulation of its expression by LuxO-LuxR regulatory system. *J. Microbiol. Biotechnol.*, **19**, 431–438.
13. Tian,Y., Wang,Q., Liu,Q., Ma,Y., Cao,X., Guan,L. and Zhang,Y. (2008) Involvement of LuxS in the regulation of motility and flagella biogenesis in *Vibrio alginolyticus*. *Biosci. Biotechnol. Biochem.*, **72**, 1063–1071.
14. Swem,L.R., Swem,D.L., Wingreen,N.S. and Bassler,B.L. (2008) Deducing receptor signaling parameters from*in vivo* analysis: LuxN/AI-1 quorum sensing in *Vibrio harveyi*. *Cell*, **134**, 461–473.
15. Timmen,M., Bassler,B.L. and Jung,K. (2006) AI-1 influences the kinase activity but not the phosphatase activity of LuxN of *Vibrio harveyi*. *J. Biol. Chem.*, **281**, 24398–24404.
16. Ye,J., Ma,Y., Liu,Q., Zhao,D.L., Wang,Q.Y. and Zhang,Y.X. (2008) Regulation of*Vibrio alginolyticus* virulence by the LuxS quorum-sensing system. *J. Fish Dis.*, **31**, 161–169.
17. Kelly,R.C., Bolitho,M.E., Higgins,D.A., Lu,W., Ng,W.L., Jeffrey,P.D., Rabinowitz,J.D., Semmelhack,M.F., Hughson,F.M. and Bassler,B.L. (2009) The *Vibrio cholerae* quorum-sensing autoinducer CAI-1: analysis of the biosynthetic enzyme CqsA. Nat. Chem. Biol., **5**, 891–895.
18. Gu,D., Liu,H., Yang,Z., Zhang,Y.X. and Wang,Q.Y. (2016) Chromatin immunoprecipitation sequencing technology reveals global regulatory roles of low-cell-density quorum-sensing regulator AphA in the pathogen *Vibrio alginolyticus*. *J. Bacteriol.*, **198**, 2985–2999.
19. Rutherford,S.T., van Kessel,J.C., Shao,Y. and Bassler,B.L. (2011) AphA and LuxR/HapR reciprocally control quorum sensing in vibrios. *Genes Dev.*, **25**, 397–408.
20. Wang,Q.Y., Liu,Q., Ma,Y., Rui,H.P. and Zhang,Y.X. (2007) LuxO controls extracellular protease, haemolytic activities and siderophore production in fish pathogen *Vibrio alginolyticus*. *J. Appl. Microbiol.*, **103**, 1525–1534.
21. Rui,H.P., Liu,Q., Ma,Y., Wang,Q.Y. and Zhang,Y.X. (2008) Roles of LuxR in regulating extracellular alkaline serine protease A, extracellular polysaccharide and mobility of *Vibrio alginolyticus*. *FEMS Microbiol. Lett.*, **285**, 155–162.
22. Cao,X., Wang,Q., Liu,Q., Liu,H., He,H. and Zhang,Y. (2010) *Vibrio alginolyticus* MviN is a*luxO*-regulated protein and affects cytotoxicity towards epithelioma papulosum cyprini (EPC) cells. *J. Microbiol. Biotechnol.*, **20**, 271–280.
23. Cao,X., Wang,Q., Liu,Q., Rui,H., Liu,H. and Zhang,Y. (2011) Identification of a *luxO*-regulated extracellular protein Pep and its roles in motility in*Vibrio alginolyticus*. *Microb. Pathog.*, **50**, 123–131.
24. Liu,H., Gu,D., Cao,X.D., Liu,Q., Wang,Q.Y. and Zhang,Y.X. (2012) Characterization of a new quorum sensing regulator *luxT* and its roles in the extracellular protease production, motility, and virulence in fish pathogen *Vibrio alginolyticus*. *Arch. Microbiol.*, **194**, 439–452.
25. Sheng,L.L., Lv,Y.Z., Liu,Q., Wang,Q.Y. and Zhang,Y.X. (2013) Connecting type VI secretion, quorum sensing, and c-di-GMP production in fish pathogen *Vibrio alginolyticus* through phosphatase PppA. *Vet. Microbiol.*, **162**, 652–662.
26. Gao,X., Wang,X., Mao,Q., Xu,R., Zhou,X., Ma,Y., Liu,Q., Zhang,Y. and Wang,Q. (2019) VqsA, a novel LysR-type transcriptional regulator, coordinates quorum sensing (QS) and is controlled by QS to regulate virulence in the pathogen *Vibrio alginolyticus*. *Appl. Environ. Microbiol.*, **84**, e00444-18.
27. Gu,D., Guo,M., Yang,M., Zhang,Y., Zhou,X. and Wang,Q. (2016) A σ^E-mediated temperature gauge controls a switch from LuxR-mediated virulence gene expression to thermal stress adaptation in *Vibrio alginolyticus*. *PLoS Pathog.*, **12**, e1005645.
28. Gibson,D.G., Young,L., Chuang,R.Y., Venter,J.C., Hutchison,C.A. 3rd and Smith,H.O. (2009) Enzymatic assembly of DNA molecules up to several hundred kilobases. *Nat. Methods.*, **6**, 343–345.
29. Juanhuix,J., Gil-Ortiz,F., Cuní,G., Colldelram,C., Nicolás,J., Lidón,J., Boter,E., Ruget,C., Ferrer,S. and Benach,J. (2014) Developments in optics and performance at BL13-XALOC, the macromolecular crystallography beamline at the ALBA synchrotron. *J. Synchrotron Radiat.*, **21**, 679–689.
30. Kabsch,W. (2010) XDS. *Acta Crystallogr. D*, **66**, 125–132.
31. Winn,M.D., Ballard,C.C., Cowtan,K.D., Dodson,E.J., Emsley,P., Evans,P.R., Keegan,R.M., Krissinel,E.B., Leslie,A.G., McCoy,A. *et al.* (2011) Overview of the CCP4 suite and current developments. *Acta Crystallogr. D*, **67**, 235–242.
32. Adams,P.D., Afonine,P.V., Bunkóczi,G., Chen,V.B., Davis,I.W., Echols,N., Headd,J.J., Hung,L.W., Kapral,G.J., Grosse-Kunstleve,R.W. *et al.* (2010) PHENIX: a comprehensive Python-based system for macromolecular structure solution. *Acta Crystallogr. D*, **66**, 213–221.
33. Emsley,P., Lohkamp,B., Scott,W.G. and Cowtan,K. (2010) Features and development of Coot. *Acta Crystallogr., D*, **66**, 486–501.
34. McCoy,A.J., Grosse-Kunstleve,R.W., Adams,P.D., Winn,M.D., Storoni,L.C. and Read,R.J. (2007) Phaser crystallographic software. *J. Appl. Crystallogr.*, **40**, 658–674.
35. Li,H. and Durbin,R. (2009) Fast and accurate short read alignment with burrows-Wheeler transform. *Bioinformatics*, **25**, 1754–1760.
36. Liang,H., Deng,X., Li,X., Ye,Y. and Wu,M. (2014) Molecular mechanisms of master regulator VqsM mediating quorum-sensing and antibiotic resistance in *Pseudomonas aeruginosa*. *Nucleic Acids Res.*, **42**, 10307–10320.
37. Feng,J.X., Liu,T., Qin,B., Zhang,Y. and Liu,X.L. (2012) Identifying ChIP-seq enrichment using MACS. *Nat. Protoc.*, **7**, 1728–1740.
38. Yang,Z., Zhou,X., Ma,Y., Zhou,M., Waldor,M.K., Zhang,Y. and Wang,Q. (2018) Serine/threonine kinase PpkA coordinates the interplay between T6SS2 activation and quorum sensing in the marine pathogen *Vibrio alginolyticus*. *Environ. Microbiol.*, **20**, 903–919.
39. Miller,D.J., Zhang,Y.M., Subramanian,C., Rock,C.O. and White,S.W. (2010) Structural basis for the transcriptional regulation of membrane lipid homeostasis. *Nat. Struct. Mol. Biol.*, **17**, 971–975.
40. Orth,P., Schnappinger,D., Hillen,W., Saenger,W. and Hinrichs,W. (2000) Structural basis of gene regulation by the tetracycline inducible Tet repressor–operator system. *Nat. Struct. Biol.*, **7**, 215–219.

41. Itou,H., Watanabe,N., Yao,M., Shirakihara,Y. and Tanaka,I. (2010) Crystal structures of the multidrug binding repressor *Corynebacterium glutamicum* CgmR in complex with inducers and with an operator. *J. Mol. Biol.*, **403**, 174–184.
42. Filippova,E.V., Wawrzak,Z., Ruan,J., Pshenychnyi,S., Schultz,R.M., Wolfe,A.J. and Anderson,W.F. (2016) Crystal structure of nonphosphorylated receiver domain of the stress response regulator RcsB from *Escherichia coli*. *Protein Sci.*, **25**, 2216–2224.
43. Schumacher,M.A., Miller,M.C., Grkovic,S., Brown,M.H., Skurray,R.A. and Brennan,R.G. (2002) Structural basis for cooperative DNA binding by two dimers of the multidrug-binding protein QacR. *EMBO J.*, **21**, 1210–1218.
44. Campanella,J.J., Bitincka,L. and Smalley,J. (2003) MatGAT: an application that generates similarity/identity matrices using protein or DNA sequences. *BMC Bioinformatics*, **4**, 29.
45. Coquant,G., Grill,J.P. and Seksik,P. (2020) Impact of N-acyl-homoserine lactones, quorum sensing molecules, on gut immunity. *Front. Immunol.*, **11**, 1827.
46. Kim,B.S., Jang,S.Y., Bang,Y.J., Hwang,J., Koo,Y., Jang,K.K., Lim,D., Kim,M.H. and Choi,S.H. (2018) QStatin, a selective inhibitor of quorum sensing in *Vibrio* species. *mBio*, **9**, e02262-17.
47. Lee,K.J., Jung,Y.C., Park,S.J. and Lee,K.H. (2018) Role of heat shock proteases in quorum-sensing-mediated regulation of biofilm formation by *Vibrio* species. *mBio*, **9**, e02086-17.
48. Brameyer,S., Plener,L., Müller,A., Klingl,A., Wanner,G. and Jung,K. (2018) Outer membrane vesicles facilitate trafficking of the hydrophobic signaling molecule CAI-1 between *Vibrio harveyi* cells. *J. Bacteriol.*, **200**, e00740-17.
49. Liu,H., Liu,W., He,X., Chen,X., Yang,J., Wang,Y., Li,Y., Ren,J., Xu,W. and Zhao,Y. (2020) Characterization of a cell density-dependent sRNA, Qrr, and its roles in the regulation of the quorum sensing and metabolism in *Vibrio alginolyticus*. *Appl. Microbiol. Biotechnol.*, **104**, 1707–1720.
50. Bagert,J.D., van Kessel,J.C., Sweredoski,M.J., Feng,L., Hess,S., Bassler,B.L. and Tirrell,D.A. (2016) Time-resolved proteomic analysis of quorum sensing in *Vibrio harveyi*. *Chem. Sci.*, **7**, 1797–1806.
51. Chaparian,R.R., Tran,M.L.N., Conrad,L.C.M., Rusch,D.B. and van Kessel,J.C. (2020) Global H-NS counter-silencing by LuxR activates quorum sensing gene expression. *Nucleic Acids Res.*, **48**, 171–183.
52. Browning,D.F. and Busby,S.J. (2016) Local and global regulation of transcription initiation in bacteria. *Nat. Rev. Microbiol.*, **14**, 638–650.
53. Ball,A.S. and van Kessel,J.C. (2019) The master quorum-sensing regulators LuxR/HapR directly interact with the alpha subunit of RNA polymerase to drive transcription activation in *Vibrio harveyi* and *Vibrio cholerae*. *Mol. Microbiol.*, **111**, 1317–1334.
54. Le,T.B., Schumacher,M.A., Lawson,D.M., Brennan,R.G. and Buttner,M.J. (2011) The crystal structure of the TetR family transcriptional repressor SimR bound to DNA and the role of a flexible N-terminal extension in minor groove binding. *Nucleic Acids Res.*, **39**, 9433–9447.
55. Zhao,Y., Zhang,G., He,C., Mei,Y., Shi,Y. and Li,F. (2018) The 11th C_2H_2 zinc finger and an adjacent C-terminal arm are responsible for TZAP recognition of telomeric DNA. *Cell Res.*, **28**, 130–134.